

A Boussinesq-scaled, pressure–Poisson water wave model



Aaron S. Donahue^{a,*}, Yao Zhang^a, Andrew B. Kennedy^a, Joannes J. Westerink^a, Nishant Panda^b, Clint Dawson^b

^a Department of Civil & Environmental Engineering & Earth Sciences, University of Notre Dame, Notre Dame, IN 46556, USA

^b Institute for Computational Engineering and Sciences, The University of Texas at Austin, Austin, TX 78712, USA

ARTICLE INFO

Article history:

Received 28 April 2014

Received in revised form 26 November 2014

Accepted 27 November 2014

Available online 13 December 2014

Keywords:

Boussinesq
Nonhydrostatic
Water waves
Phase resolving
Green Naghdi
Pressure Poisson

ABSTRACT

Through the use of Boussinesq scaling we develop and test a model for resolving non-hydrostatic pressure profiles in nonlinear wave systems over varying bathymetry. A Green–Naghdi type polynomial expansion is used to resolve the pressure profile along the vertical axis, this is then inserted into the pressure–Poisson equation, retaining terms up to a prescribed order and solved using a weighted residual approach. The model shows rapid convergence properties with increasing order of polynomial expansion which can be greatly improved through the application of asymptotic rearrangement. Models of Boussinesq scaling of the fully nonlinear $O(\mu^2)$ and weakly nonlinear $O(\mu^N)$ are presented, the analytical and numerical properties of $O(\mu^2)$ and $O(\mu^4)$ models are discussed. Optimal basis functions in the Green–Naghdi expansion are determined through manipulation of the free-parameters which arise due to the Boussinesq scaling. The optimal $O(\mu^2)$ model has dispersion accuracy equivalent to a Padé [2,2] approximation with one extra free-parameter. The optimal $O(\mu^4)$ model obtains dispersion accuracy equivalent to a Padé [4,4] approximation with two free-parameters which can be used to optimize shoaling or nonlinear properties. In comparison to experimental results the $O(\mu^4)$ model shows excellent agreement to experimental data.

© 2014 The Authors. Published by Elsevier Ltd. This is an open access article under the CC BY-NC-ND license (<http://creativecommons.org/licenses/by-nc-nd/3.0/>).

1. Introduction

Boussinesq type models have been used to make numerical predictions about nearshore wave phenomenon since their introduction by Peregrine (1967) and Madsen and Mei (1969). Through the use of a Boussinesq-type nondimensional scaling approach it was possible to design a relatively simple model which was applicable for shallow water waves, $\mu = kh \leq \pi/2$. Early models were weakly dispersive and weakly nonlinear, limiting their applicability in deeper water. Work by Madsen et al. (1991), Madsen and Srensen (1992) and Nwogu (1993) demonstrated that with careful manipulation of the equations it was possible to generate models with better dispersion characteristics, formally up to $O(\mu^4)$. Further work incorporated higher-order solutions with increased accuracy in shoaling and nonlinear interactions (Agnon et al., 1999; Kennedy et al., 2001; Schäffer and Madsen, 1995; Wei et al., 1995) and more relevant physics to the nearshore such as wave breaking and wave run-up (Chen et al., 2000; Kennedy et al., 2000; Lynett et al., 2002; Schäffer et al., 1993). The work of Gobbi and Kirby (2001), Gobbi

et al. (2000) and Madsen and Schäffer (1998) extended the order of accuracy of the models, obtaining a dispersive relationship that was formally of $O(\mu^8)$, thereby expanding the range over which valid solutions could be obtained. Taking a different approach, Lynett and Liu (2004a,b) examined the increased accuracy gained through solutions to Boussinesq models over multiple vertical layers. The use of multiple layers provided an increase in the number of free-parameters which could be used to improve the model accuracy. Building on the advances made in Serre–Green–Naghdi type modeling of water waves (Bonneton et al., 2011; Green and Naghdi, 1976; Serre, 1953), Zhang et al. (2013, 2014) were able to obtain an equivalent formal high-order of accuracy, even for low-order models, through the use of Green–Naghdi type polynomial expansions over the vertical domain for the velocities and the use of asymptotic rearrangement to find the optimal vertical basis functions.

Many of the higher-order models came at the cost of model complexity, which in many cases hindered the potential for these models to be adopted on a large scale. With the exception of Zhang et al. (2013), in order to obtain formally higher-order models it was necessary to use higher order spatial derivatives, which increases the computational cost. In addition mixed space/time derivatives are inherent in Boussinesq type models, see Peregrine (1967). Mixed

* Corresponding author.

E-mail address: adonahu1@nd.edu (A.S. Donahue).

space/time can be computationally expensive and difficult to implement, especially in two horizontal dimensions.

Wei and Kirby (1995) suggested the use of a higher-order Adams–Bashforth–Moulton predictor–corrector time integration scheme, thus ensuring that the dispersive error dominated the truncation error in the temporal discretization. Following their work and owing to the potential for greater spatial accuracy for lower computational cost hybrid spatial finite volume finite difference (Erduran et al., 2005; Shi et al., 2012; Gallerano et al., 2014) and finite element (Do Carmo et al., 1993; Li et al., 1999; Panda et al., 2014) implementations of the Boussinesq equations have been developed, these methods either employed higher-order predictor–corrector methods in time or took advantage of higher-order Runge–Kutta (RK) or Strong-Stability-Preserving-Runge–Kutta (SSPRK) methods in time. Furthermore, rearrangement of the dispersive terms such that the numerical solution of the one horizontal dimension model only requires the solution of a tridiagonal system addressed the computational cost issue associated with mixed space/time derivatives. However, in two horizontal dimensions it is still necessary to solve a set of two tightly coupled systems of equations.

Recently focus has shifted towards resolution of the dispersive terms through the solution of the Poisson type problems. This approach reduces the system to only one unknown, the pressure profile, in two-horizontal dimensions, as opposed to a set of two coupled velocity problems. A novel approach has been introduced by Antuono and Brocchini (2013) which focuses on solutions to a Poisson equation in the vertical velocity. This is achieved through a decomposition of the horizontal velocities into two parts, a depth-averaged velocity component and a deviation from depth-averaged term. The latter is further decomposed into rotational and irrotational components. Manipulation of the vorticity equations and the continuity equation yields a Poisson type problem, which when solved informs the deviation of the horizontal velocity from the depth-averaged component.

An approach that has recently gained traction is the resolution of dispersive effects by focusing on the non-hydrostatic pressure term. Building upon the concept introduced by Casulli and Stelling (1998), Casulli (1999) and Stansby and Zhou (1998) many highly accurate models have been developed and tested. Examples include the work of Yamazaki et al. (2009) on a depth integrated non-hydrostatic model, the Simulating WAVes till SHore (SWASH) model developed by Stelling and Zijlema (2003), Zijlema and Stelling (2008) and Zijlema et al. (2011), the Non Hydrostatic WAVE (NHWAVE) model developed by Ma et al. (2012) and the CCHE2D model of Wei and Jia (2013). Each of these models have focused on solutions to the shallow water equations (SWE) or full Navier–Stokes equations where the non-hydrostatic pressure is treated as a single unknown which must be found numerically. The result is a model that does not include any mixed space/time derivatives, they do however involve an extra pressure–Poisson problem which must be solved to determine the non-hydrostatic pressure.

Zijlema and Stelling (2005) were able to demonstrate numerically that with an increased number of vertical layers it was possible to obtain high order accuracy for the dispersion characteristics. More recently Bai and Cheung (2013) derived the dispersion relationship and shoaling coefficient for the single and two layer models, as well as a more accurate hybrid single layer model. The results of the linear dispersion analysis for the single layer showed that it was only accurate for very shallow water waves. The more expensive two layer model demonstrated a significant improvement, equivalent to a Padé [2,4] approximation to the Airy solution, while the single layer hybrid model contained a free-parameter that could be used to optimize the dispersion to a Padé [2,2] approximation.

A separate approach based on an extension of the SWE's to include dispersive effects while retaining their hyperbolic structure has been proposed by Antuono et al. (2009). Assuming a sufficiently smooth bathymetry these so called Dispersive Nonlinear Shallow Water Equations (DNSWE's) are able to remain strictly hyperbolic through the inclusion of two pseudo-potential functions, thus they can take advantage of higher order finite volume or finite element numerical methods (Grosso et al., 2010).

The coupling of Boussinesq-type models with oceanographic models was stated as improvement of high urgency by Brocchini (2013) in his comprehensive analysis of the current state of Boussinesq models. The present work aims to take the advances made in classical Boussinesq theory and the recent work in multi-layer non hydrostatic pressure models to design a Boussinesq type model for the non-hydrostatic pressure which is suitable for a straightforward coupling with oceanographic models. Instead of vertical layers, a Green–Nagdhi type polynomial expansion is used to resolve the pressure over the vertical domain. The result is a simple model for the non-hydrostatic pressure, which is found through the solution to the pressure–Poisson equation and enforcement of the bottom boundary condition on pressure. The combination of a Green–Nagdhi type polynomial expansion with Boussinesq-type scaling provides free-parameters, which can be manipulated using the principles of asymptotic rearrangement to optimize for various properties including dispersion, shoaling and nonlinear interactions. At lowest-order the model is comparable to standard Boussinesq models as well as the hybrid single layer model of Bai and Cheung (2013) At higher-order the model compares well with the higher order models of Gobbi and Kirby (1999) and Zhang et al. (2013), but is relatively easier to implement and does not contain higher-order spatial derivatives or mixed space/time derivatives.

This paper is organized as follows: Section 2 introduces the dimensionless scaling and the governing equations for the model. In Section 3 a pressure–Poisson model using Boussinesq scaling and Green–Nagdhi type expansions in the vertical axis is developed. Section 4 discusses the analytical properties of the model and compares them with well known analytical results. Section 5 discusses several validation experiments conducted using a numerical solution to the model. Finally the conclusions of the paper are given in Section 6. Appendix A provides details of reduction in the degrees of freedom for higher order solutions, appendix B provides details of the linear dispersion and shoaling analysis and appendix C provides details of the nonlinear analysis for the second order nonlinear term.

2. Scaling

For the present study we will consider flow of a constant density inviscid fluid without bottom or surface shear stresses. We employ a Cartesian coordinate system (x^*, y^*, z^*) , where z^* represents the vertical axis centred on the still-water plane pointing upwards. The full vertical profile stretches from the bottom bathymetry at $z^* = -h^*(x^*, y^*)$ to the free-surface $z^* = \eta^*(x^*, y^*, t^*)$. The following nondimensional quantities are defined:

$$\begin{aligned} (x, y) &= k_0(x^*, y^*), & (u, v) &= \frac{h_0}{a_0 \sqrt{g_0 h_0}}(u^*, v^*), \\ \eta &= \frac{\eta^*}{a_0}, & z &= \frac{z^*}{h_0}, \\ w &= \frac{w^*}{a_0 k_0 \sqrt{g_0 h_0}}, & P &= \frac{P^*}{\rho g_0 a_0}, \\ h &= \frac{h^*}{h_0}, & g &= \frac{g^*}{g_0}, \\ t &= k_0 \sqrt{g_0 h_0} t^*, \end{aligned} \quad (1)$$

where the superscript * denotes a dimensional variable. The variables u , v and w represent the velocities in the x , y and z directions respectively. The pressure, P , is defined over the entire fluid domain and the free-surface elevation, η , is defined over the horizontal axis (x, y) . The variable h represents the bathymetric depth, g is the non-dimensional gravitational constant and t represents time. The parameters k_0, h_0, g_0, a_0 and ρ stand for a reference wavenumber, reference bathymetric depth, the gravitational constant, a reference wave amplitude and the fluid density, respectively.

2.1. Governing equations

Inserting the scaled parameters into the conservation of momentum equations, we obtain the following nondimensional forms of the conservation of momentum equations for incompressible inviscid fluid motion,

$$\frac{\partial \mathbf{u}}{\partial t} + \delta \nabla \cdot (\mathbf{u}\mathbf{u}^T) + \delta \frac{\partial}{\partial z} (w\mathbf{u}) + \nabla P = \mathbf{0}, \quad -h \leq z \leq \delta\eta, \quad (2)$$

$$\mu^2 \frac{\partial w}{\partial t} + \delta \mu^2 \nabla \cdot (\mathbf{u}w) + \delta \mu^2 \frac{\partial}{\partial z} (w^2) + \frac{\partial P}{\partial z} + \frac{g}{\delta} = 0, \quad -h \leq z \leq \delta\eta, \quad (3)$$

where $\mu \equiv k_0 h_0$ is a measure of frequency dispersion, $\delta \equiv a_0/h_0$ is a measure of nonlinearity, $\nabla \equiv (\partial/\partial x, \partial/\partial y)^T$ is the two-dimensional gradient operator and $\mathbf{u} \equiv (u, v)^T$ is the horizontal velocity vector. The nondimensional forms of the continuity equation and the kinematic free-surface and bottom boundary conditions are given as,

$$\nabla \cdot \mathbf{u} + \frac{\partial w}{\partial z} = 0, \quad -h \leq z \leq \delta\eta, \quad (4)$$

$$w - \frac{\partial \eta}{\partial t} - \delta \mathbf{u} \cdot \nabla \eta = 0, \quad z = \delta\eta, \quad (5)$$

$$w + \mathbf{u} \cdot \nabla h = 0, \quad z = -h. \quad (6)$$

Taking the divergence of the conservation of momentum equations, Eqs. (2) and (3), and considering the continuity equation, Eq. (4), the pressure-Poisson equation is derived with the same scaling quantities,

$$\mu^2 \nabla^2 P + \frac{\partial^2 P}{\partial z^2} = -\delta \mu^2 \nabla^{(3)} \cdot (\mathbf{u}^{(3)} \cdot \nabla^{(3)} \mathbf{u}^{(3)}), \quad -h \leq z \leq \delta\eta, \quad (7)$$

where $\nabla^{(3)} \equiv (\partial/\partial x, \partial/\partial y, \partial/\partial z)$ and $\mathbf{u}^{(3)} \equiv (u, v, w)$. Integrating Eq. (4) over the vertical domain from the bathymetric depth, $z = -h$, to the free-surface, $z = \delta\eta$ and applying the kinematic boundary conditions derives an expression for the conservation of mass dependent on the free-surface elevation and the fluid flux,

$$\frac{\partial \eta}{\partial t} + \nabla \cdot \int_{-h}^{\delta\eta} \mathbf{u} dz = 0. \quad (8)$$

Similarly, considering Eq. (3) at $z = -h$ and applying the kinematic bottom boundary condition, Eq. (6), the bottom pressure boundary condition is obtained,

$$\mu^2 (\nabla h) \cdot (\nabla P) + \frac{\partial P}{\partial z} + \frac{g}{\delta} = \delta \mu^2 \mathbf{u} \cdot (\mathbf{u} \cdot \nabla^2 h), \quad z = -h. \quad (9)$$

Eqs. (2), (3), (7), (8) and (9) make up the complete set of governing equations that will be solved in this work. The pressure field for a particular velocity field $\mathbf{u}^{(3)}$, and free-surface displacement, $\delta\eta$, at time t can be derived from Eqs. (7) and (9). Once the pressure field has been determined, the time evolution of the velocity field $\mathbf{u}^{(3)}$ can be realized by substitution of the pressure field, P , into Eqs. (2) and (3). In addition, the time evolution of the free-surface is realized by substitution of the velocity field into Eq. (8). High-order models are constructed through application of Boussinesq-type approximations to the dependent variables; \mathbf{u} , w and P . The classic approach in Boussinesq models is to find a solution for the pressure in terms of the horizontal and vertical velocity profiles and then substitute this solution into the conservation of momentum or

velocity potential equations. This produces a system of equations based entirely on the free-surface and the velocities, but as mentioned previously this also requires solutions to mixed space/time derivatives.

The present work focuses on the derivation of an independent pressure model which does not include any mixed space/time derivatives. Similarly, the use of a single Poisson type model to resolve the dispersive terms will yield a model which with fewer terms and a simpler form when compared with Boussinesq-type models of equal order.

2.2. Pressure expansion

We begin by considering the standard approach to solving for the pressure profile in Boussinesq theory. Integrating Eq. (3) from an arbitrary depth, z , to the free-surface and applying the zero free-surface pressure condition, an expression for the vertical pressure profile in terms of the horizontal and vertical velocities is obtained,

$$P = \frac{g}{\delta} (\delta\eta + h)(1 - q) + \mu^2 \int_z^{\delta\eta} \left(\frac{\partial w}{\partial t} + \delta \nabla \cdot (\mathbf{u}w) + \delta \frac{\partial}{\partial z} (w^2) \right) dz, \quad (10)$$

where the variable sigma coordinate $q \in [0, 1]$, defined as

$$q \equiv \frac{z + h}{\delta\eta + h} \quad (11)$$

has been introduced to simplify the equations. In this work we consider the Boussinesq approximation for the velocity expanded about the depth-averaged velocity, $\bar{\mathbf{u}}$. This was the approach first used by Peregrine (1967) and later by Madsen and Schäffer (1998), and others. The horizontal and vertical velocities are given by,

$$\begin{aligned} \mathbf{u} = & \bar{\mathbf{u}} + \mu^2 (\nabla (\nabla \cdot (h\bar{\mathbf{u}})) - h \nabla (\nabla \cdot \bar{\mathbf{u}})) (\delta\eta + h) \left(\frac{1}{2} - q \right) \\ & + \mu^2 \left(\frac{1}{2} (\delta\eta + h)^2 \nabla (\nabla \cdot \bar{\mathbf{u}}) \right) \left(\frac{1}{3} - q^2 \right) \\ & + \mu^4 \mathbf{u}_3 \left(\frac{1}{4} - q^3 \right) + \mu^4 \mathbf{u}_4 \left(\frac{1}{5} - q^4 \right) + O(\mu^6) \end{aligned} \quad (12)$$

and,

$$w = -\bar{\mathbf{u}} \cdot \nabla h - (h + \delta\eta) (\nabla \cdot \bar{\mathbf{u}}) q + O(\mu^2), \quad (13)$$

where \mathbf{u}_3 and \mathbf{u}_4 are complicated differential functions of $\bar{\mathbf{u}}$, for more detail see Madsen and Schäffer (1998). Substitution of Eqs. (12) and (13) into Eq. (10) provides an expression for the pressure profile, which includes the typical mixed space/time derivatives, i.e. $\partial/\partial t (\nabla \cdot \bar{\mathbf{u}})$. With a simple rearrangement of terms it is possible to construct a general formula for the pressure profile which includes a Green-Nagdhi type polynomial expansion in the vertical axis,

$$P = P_0 + \sum_{n=1}^N \mu^{\beta_n} P_n \phi_n + O(\mu^{N+2}), \quad (14)$$

where $\beta_n = n + n_{\text{mod}} 2$ is equal to n when n is even and equal to $n + 1$ when n is odd, $P_0 = P_0(\mathbf{x}, t, q)$ is the zeroth-order component of the expansion, $P_n = P_n(\mathbf{x}, t)$ is the n th term in the expansion, and the vertical basis functions $\phi_n = \phi_n(q)$ are defined in such a way that the zero free-surface pressure condition is explicitly satisfied,

$$\phi_n = \sum_{m=1}^n \hat{\phi}_{mn} (1 - q^m), \quad (15)$$

where the $\hat{\phi}_{mn}$ are arbitrary constants, and $\hat{\phi}_{mn} = 1$ can be assumed without loss of generality.

It is noted that the use of polynomial expansions leads to a limited region of accuracy in the dispersion and shoaling relationship (Madsen and Agnon, 2003). This will be discussed in further detail in Section 4, where it will be demonstrated that the approximate dispersion and shoaling relationships converge to the analytical solution of linear theory as the number of terms in the polynomial expansion is increased, and that with the appropriate choice of basis function it is possible to expand the valid range of the model to well beyond the region of interest even at low-order. It is noted that in order to derive a pressure expansion with terms up to q^N it is necessary to apply a velocity expansion out to an equivalent number of terms q^N . The theoretical framework for obtaining higher order expansions has been outlined by Madsen and Schäffer (1998), among others.

In the following sections a strategy for determining each of the P_n terms will be developed. It will be shown that the solution for the pressure profile does not involve any mixed space/time derivatives, has few degrees of freedom to solve for, and with the appropriate choice of basis functions ϕ_n can produce highly accurate solutions.

3. A Boussinesq-type non-hydrostatic pressure-Poisson model

Although expressions for the P_n terms in the pressure expansion can be determined through substitution of the Boussinesq approximations for the horizontal and vertical velocities into the vertical conservation of momentum equation, see Eq. (10), these expressions often involve higher order spatial derivatives and mixed space/time derivatives (Nwogu, 1993). Alternatively, we discuss an approach for determining the pressure expansion terms where they are treated as unknowns which are found as a solution to the pressure-Poisson equation and the bottom boundary condition for pressure, Eqs. (7) and (9). The weighted residual method is utilized in order to generate a sufficient number of equations to match the order of the desired pressure expansion. The result is a set of equations equal in number to the order of the expansion which include spatial derivatives of at most second-order, and no mixed space/time derivatives.

The general form of the pressure solution follows Eq. (14). Through the course of this work it was determined that the solution to the pressure profile was dependent on the choice of approximation for the zeroth-order term, P_0 . A direct integration of the vertical momentum equation provides an expansion about the hydrostatic pressure, which gives,

$$P = \frac{g}{\delta}(\delta\eta + h)(1 - q) + \sum_{n=1}^N \mu^{\beta_n} \phi_n P_n + O(\mu^{N+2}). \quad (16)$$

However, the solution to the pressure for this choice of P_0 led to undesirable overall properties, which will be discussed in Section 4. If the zeroth-order term in the expansion is taken to be the still water pressure term, as in Peregrine (1967), the model exhibits more desirable properties in terms of dispersion characteristics. This particular expansion can be derived in the same manner through a simple rearrangement of terms. Considering Eq. (16), we rearrange the terms to obtain

$$P = \frac{g}{\delta} h(1 - q) + \overbrace{(g\eta + \mu^2 P_1)}^{\tilde{P}_1} (1 - q) + \sum_{n=2}^N \mu^{\beta_n} P_n \phi_n + O(\mu^{N+2}), \quad (17)$$

where $\frac{g}{\delta} h(1 - q)$ represents the pressure for a fluid at rest and \tilde{P}_1 is an $O(1)$ pressure correction term. Note that this expression is equivalent to the expansion given by Eq. (16) and that all the remaining terms in the pressure expansion remain unchanged. Dropping the \sim notation leads to the general solution for pressure,

$$P = \frac{g}{\delta} h(1 - q) + P_1(1 - q) + \sum_{n=2}^N \mu^{\beta_n} P_n \phi_n + O(\mu^{N+2}). \quad (18)$$

Eq. (18) defines the general N^{th} order Boussinesq-type approximation to the pressure.

Given a desired order of accuracy in the model, an initial free-surface displacement, and set of horizontal velocities, the process for determining the non-hydrostatic pressure profile and updating the free-surface and velocities is as follows:

1. Determine the desired order of accuracy, $O(\mu^N)$.
2. Insert the velocity profile, Eqs. (12) and (13), into Eqs. (7) and (9) to generate a system of pressure-Poisson equations for the pressure.
3. Substitute the Boussinesq approximation to the pressure profile Eq. (18) and the free-surface elevation into the system of pressure-Poisson equations generated in step 2.
4. Discard any terms that are formally greater than the desired order.
5. Apply the weighted residual method over the vertical axis in order to generate a sufficient number of equations to match the number of unknown terms in the pressure expansion.
6. Solve the system of equations from step 5 for the unknown pressure expansion terms P_n , for $n = 1 \dots N$.
7. Substitute the Boussinesq-type approximation for the pressure profile from step 6 and the velocities into the depth-integrated form of Eq. (2) and (8) to advance the horizontal velocities and free-surface forward in time. Furthermore substitution of the horizontal velocities into Eq. (13) determine the vertical velocity, w .

3.1. Boussinesq system of equations with no mixed space-time derivatives

We consider a Boussinesq type expansion of the pressure field with scaling up to order $O(\mu^N)$. The horizontal velocities, \mathbf{u} , and vertical velocity, w , are given by Eqs. (12) and (13). The Boussinesq-type expansion for the pressure, P , is given by Eq. (18). Note that the basis functions for pressure, Eq. (15), are defined such that they disappear at the free-surface, $q = 1$, thus the zero pressure free-surface boundary condition is explicitly satisfied. Substituting Eq. (18) into Eq. (7) produces an expression for the pressure-Poisson equation,

$$\begin{aligned} & \sum_{n=1}^N \mu^{\beta_n} \left[\mu^2 \phi_n \nabla^2 P_n + 2\mu^2 \phi_n' \nabla q \cdot \nabla P_n \right. \\ & \left. + \left(\phi_n'' \left(\mu^2 (\nabla q) \cdot (\nabla q) + \left(\frac{\partial q}{\partial z} \right)^2 \right) + \mu^2 \phi_n' \nabla^2 q \right) P_n \right] \\ & = -\mu^2 \delta^2 \nabla^3 \cdot (\mathbf{u}^{(3)} \cdot \nabla^3 \mathbf{u}^{(3)}) - \mu^2 \frac{g}{\delta} (\nabla^2 h(1 - q) - 2(\nabla h) \cdot (\nabla q) - h \nabla^2 q) \\ & + O(\mu^{N+2}), 0 \leq q \leq 1. \end{aligned} \quad (19)$$

Similarly, substitution into Eq. (9) produces an expression for the pressure bottom boundary condition,

$$\begin{aligned} & \sum_{n=1}^N \mu^{\beta_n} (\mu^2 (h + \delta\eta) \phi_n \nabla h \cdot \nabla P_n + (1 + \mu^2 (\nabla h) \cdot (\nabla h)) \phi_n' P_n) \\ & = \delta \mu^2 (h + \delta\eta) \mathbf{u} \cdot (\mathbf{u} \cdot \nabla^2 h) - g(1 + \mu^2 (\nabla h) \cdot (\nabla h)) \eta \\ & + O(\mu^{\beta_n+2}), q = 0. \end{aligned} \quad (20)$$

Since there are N unknowns, P_n , and only two equations, a weighted residual in the vertical direction is used to solve the full system for the pressure-Poisson component of the equations. Arbitrary weighting functions were employed in order to determine if the choice of weighting function influenced the solution. As will

be illustrated in the case for a two term expansion, i.e. $N = 2$, the choice of weighting functions has a direct impact on the solution accuracy and stability. The weighting functions are defined as follows,

$$W_n = \sum_{m=0}^n \widehat{W}_{mn} q^m, \quad \widehat{W}_{nn} = 1, \quad (21)$$

where \widehat{W}_{mn} are constants to be determined, and the set of weighting functions is linearly independent. Each equation in the weighted residual method takes the form,

$$\begin{aligned} & \int_0^1 W_m \left(\sum_{n=1}^N \mu^{\hat{\beta}_n} \left[\mu^2 \phi_n \nabla^2 P_n + 2\mu^2 \phi_n' \nabla q \cdot \nabla P_n \right. \right. \\ & \left. \left. + \left(\phi_n'' \left(\mu^2 (\nabla q) \cdot (\nabla q) + \left(\frac{\partial q}{\partial z} \right)^2 \right) + \mu^2 \phi_n' \nabla^2 q \right) P_n \right] \right) dq \\ & = \int_0^1 W_m \left(-\mu^2 \delta^2 \nabla^{(3)} \cdot (\mathbf{u}^{(3)} \cdot \nabla^{(3)} \mathbf{u}^{(3)}) \right. \\ & \left. - \mu^2 \frac{g}{\delta} \left(\nabla^2 h(1-q) - 2(\nabla h) \cdot (\nabla q) - h \nabla^2 q \right) \right) dq + O(\mu^{\hat{\beta}_n+2}) \end{aligned} \quad (22)$$

for $m = 1 \dots N-1$.

The system of equations comprised of Eqs. (20) and (22) are solved to determine all P_n , which in turn determines the pressure profile that can then be used with the conservation of momentum equations to update the velocities.

Substitution of the velocity expansion, Eq. (12), demonstrates that the conservation of mass, Eq. (8), is only dependent on the depth-averaged velocity,

$$\eta_{,t} + \nabla \cdot ((\delta\eta + h)\bar{\mathbf{u}}) = 0. \quad (23)$$

In order to update the horizontal velocities we consider the depth integral of Eq. (2),

$$\int_{-h}^{\delta\eta} \left[\frac{\partial \mathbf{u}}{\partial t} + \delta \nabla \cdot (\mathbf{u}\mathbf{u}^T) + \delta \frac{\partial}{\partial z} (\mathbf{w}\mathbf{u}) + \nabla P \right] dz = 0. \quad (24)$$

Application of the Leibniz integration rule and the kinematic free-surface and bottom boundary conditions yields the following simplification of Eq. (24),

$$\frac{\partial}{\partial t} \int_{-h}^{\delta\eta} \mathbf{u} dz + \delta \nabla \cdot \int_{-h}^{\delta\eta} (\mathbf{u}\mathbf{u}^T) dz + \int_{-h}^{\delta\eta} (\nabla P) dz = 0, \quad (25)$$

see Nwogu equations (12) and (13) (Nwogu, 1993). It is clear from the definition of the velocity profile expansion, Eq. (12), that at $O(\mu^2)$ only the zeroth order velocity terms are retained in Eq. (25), thus,

$$\frac{\partial}{\partial t} ((h + \delta\eta)\bar{\mathbf{u}}) + \delta \nabla \cdot ((h + \delta\eta)\bar{\mathbf{u}}\bar{\mathbf{u}}^T) + \int_{-h}^{\delta\eta} (\nabla P) dz + O(\delta\mu^4) = 0. \quad (26)$$

Substitution of the pressure expansion, Eq. (18), the conservation of mass, Eq. (23), and division by $(h + \delta\eta)$, yields the final form of the horizontal momentum equation in vector notation,

$$\begin{aligned} & \frac{\partial \bar{\mathbf{u}}}{\partial t} + \delta \bar{\mathbf{u}} \cdot \nabla \bar{\mathbf{u}} + \sum_{n=0}^N \mu^{\hat{\beta}_n} \left(G_n \nabla P_n - \frac{1}{h + \delta\eta} \left(\phi_n|_{q=0} \nabla h + R_n \nabla (h + \delta\eta) \right) P_n \right) \\ & + O(\mu^{N+2}, \delta\mu^4) = 0, \end{aligned} \quad (27)$$

where G_n and R_n are given in Table 1, and evaluated at $q = 1$. It is important to note that based on the definition of the depth averaged velocity, the first term in Eq. (27) is linearly exact for all orders, while the convective term is exact up to $O(\mu^2)$, with errors of $O(\delta\mu^4)$. Given a pressure profile expansion of $O(\mu^N)$, we have either a fully nonlinear $O(\mu^2)$ or weakly nonlinear $O(\mu^N)$, $N > 2$, model which is only dependent on the depth-averaged horizontal velocities.

Table 1
Definition of Integrals.

$\Psi_{nm} = \int_0^q W_m \hat{q} \phi_n'' d\hat{q}$	$\Phi_{nm} = \int_0^q W_m \hat{q} \phi_n' d\hat{q}$	$\Omega_m = \int_0^q W_m d\hat{q}$
$G_n = \int_0^q \phi_n d\hat{q}$	$R_n = \int_0^q \hat{q} \phi_n' d\hat{q}$	$\xi_{nm} = \int_0^q W_m \phi_n d\hat{q}$
$\Gamma_{nm} = \int_0^q W_m \hat{q} \phi_n d\hat{q}$	$\chi_m = \int_0^q W_m \hat{q} d\hat{q}$	$S_{nm} = \int_0^q W_m \hat{q}^2 \phi_n'' d\hat{q}$
$\Theta_{nm} = \int_0^q W_m \phi_n' d\hat{q}$	$\Lambda_{nm} = \int_0^q W_m \phi_n'' d\hat{q}$	

Eqs. (20), (22), (23) and (27) make up the complete system of equations for the model. Recall that the solution for w is explicitly defined in terms of $\bar{\mathbf{u}}$ by Eq. (13). Having the pressure model only rely on the depth-integrated velocity is advantageous in that some ocean circulation models assume a depth-averaged velocity, thus all conclusions about increased accuracy from the inclusion of a non-hydrostatic pressure model can be extended to the general class of ocean circulation models. The equations for pressure are an elliptic problem, while the equations for velocity and the free-surface are both hyperbolic. The strategy for solving this system of equations has two steps:

1. Given a specific velocity and free-surface profile, determine the pressure profile using Eqs. (20) and (22).
2. Update the velocities and free-surface using Eqs. (27) and (23) using the pressure profile found in the previous step. Recall that the Boussinesq expansion for the vertical velocity, w , is represented in terms of the depth averaged horizontal velocity.

3.2. Fully nonlinear $O(\mu^2)$ solution

Substituting the horizontal and vertical velocities, Eqs. (12) and (13), into the governing equations for the pressure solution, Eqs. (20) and (22), and truncating all terms of order greater than $O(\mu^2)$ produces a system of equations to solve for the pressure expansion components, P_1 and P_2 .

Bottom boundary condition:

$$a_{1,2} P_2 + a_{2,1} \cdot \nabla P_1 + a_{1,1} P_1 = a_0 + O(\mu^4), \quad (28)$$

where,

$$a_{1,2} = \left(\mu^2 \hat{\phi}_{12} \right), \quad (29)$$

$$a_{2,1} = -(\mu^2 (h + \delta\eta) (\nabla h)), \quad (30)$$

$$a_{1,1} = ((1 + \mu^2 (\nabla h) \cdot (\nabla h))), \quad (31)$$

$$a_0 = g \left(1 + \mu^2 (\nabla h)^2 \right) \eta - \delta \mu^2 (h + \delta\eta) \bar{\mathbf{u}} \cdot (\bar{\mathbf{u}} \cdot \nabla^2 h) \quad (32)$$

and

Pressure-Poisson:

$$b_{1,2,1} P_2 + b_{3,1,1} \nabla^2 P_1 + b_{2,1,1} \cdot \nabla P_1 + b_{1,1,1} P_1 = b_{0,1} + O(\mu^4), \quad (33)$$

where,

$$b_{1,2,1} = -\mu^2 \omega_1, \quad (34)$$

$$b_{3,1,1} = \frac{1}{6} \mu^2 \omega_2 (h + \delta\eta)^2, \quad (35)$$

$$b_{2,1,1} = \frac{1}{3} \mu^2 ((1 + \omega_2) \delta \nabla \eta - \omega_2 \nabla h) (h + \delta\eta), \quad (36)$$

$$\begin{aligned} b_{1,1,1} = & -\frac{1}{6} \mu^2 \left[(\omega_2 \nabla^2 h - \delta(1 + \omega_2) \nabla^2 \eta) (h + \delta\eta) \right. \\ & \left. + 2((1 + \omega_2) \delta \nabla \eta - \omega_2 \nabla h) \cdot \nabla (h + \delta\eta) \right], \end{aligned} \quad (37)$$

$$\begin{aligned} b_{0,1} = & -\frac{1}{2} \delta \mu^2 \omega_1 (h + \delta\eta)^2 \nabla \cdot (\bar{\mathbf{u}} \cdot \nabla \bar{\mathbf{u}}) - \frac{1}{6} g \mu^2 (1 + \omega_2) (h + \delta\eta) h \nabla^2 \eta \\ & - \frac{1}{3} g \mu^2 (\delta(1 + \omega_2) (\eta \nabla h - h \nabla \eta) + \omega_2 h \nabla h) \cdot \nabla \eta \\ & - \frac{1}{6} g \mu^2 \omega_2 \left((h + \delta\eta) \nabla^2 h - 2(\nabla h) \cdot (\nabla h) \right) \eta, \end{aligned} \quad (38)$$

where $\omega_1 = (1 + 2\widehat{W}_{01})$ and $\omega_2 = (1 + 3\widehat{W}_{01})$ are defined in order to simplify the expressions and with $W_1 = \widehat{W}_{01} + q$ as the arbitrary weighting function used in the weighted residual approach. Simultaneous solutions of Eqs. (28) and (33) determines the pressure profile components, P_1 and P_2 . The pressure and velocity expansions are substituted into the horizontal velocity and conservation of mass equations, Eqs. (27) and (23), to advance the velocities and free-surface forward in time as follows,

$$\begin{aligned} \frac{\partial \bar{\mathbf{u}}}{\partial t} + \delta \bar{\mathbf{u}} \cdot \nabla \bar{\mathbf{u}} + \frac{1}{2} \mathbf{g} \left(\frac{h(\nabla \eta) + (\nabla h)\eta}{h + \delta \eta} \right) + \frac{1}{6} \mu^2 (4 + 3\hat{\phi}_{12}) \nabla P_2 \\ + \frac{1}{6} \mu^2 \left(\frac{\delta(4 + 3\hat{\phi}_{12}) \nabla \eta - (2 + 3\hat{\phi}_{12}) \nabla h}{h + \delta \eta} \right) P_2 \\ + \frac{1}{2} \nabla P_1 + \frac{1}{2} \left(\frac{\delta \nabla \eta - \nabla h}{h + \delta \eta} \right) P_1 + O(\mu^4) = 0 \end{aligned} \quad (39)$$

and

$$\frac{\partial \eta}{\partial t} + \nabla((h + \delta \eta) \bar{\mathbf{u}}) = 0. \quad (40)$$

3.2.1. Reduction in the degrees of freedom for the fully nonlinear $O(\mu^2)$ case

It is possible to reduce the degrees of freedom in the overall system. We first note that P_2 can be solved for explicitly in terms of P_1 and ∇P_1 through algebraic manipulation of Eq. (28),

$$P_2 = \frac{1}{a_{1,2}} (a_0 - a_{2,1} \cdot \nabla P_1 - a_{1,1} P_1) + O(\mu^4), \quad (41)$$

provided $a_{1,2} \neq 0$. Substituting Eq. (41) into Eq. (33), a single elliptic problem for P_1 is obtained,

$$\begin{aligned} b_{3,1,1} \nabla^2 P_1 + \left(b_{2,1,1} - \frac{b_{1,2,1}}{a_{1,2}} a_{2,1} \right) \cdot \nabla P_1 \\ + \left(b_{1,1,1} - \frac{b_{1,2,1}}{a_{1,2}} a_{1,1} \right) P_1 \\ = \left(b_{0,1} - \frac{b_{1,2,1}}{a_{1,2}} a_0 \right) + O(\mu^4), \end{aligned} \quad (42)$$

where all the coefficients are defined as above. In one horizontal dimension Eq. (42) results in a tri-diagonal matrix to solve the linear system. Similar to standard Boussinesq models, extension into two horizontal dimensions will necessitate the use of iterative techniques to solve the linear system in a computationally efficient manner, however unlike standard Boussinesq theory, which has an elliptic problem associated with each of the horizontal velocities, the model has only one elliptic problem which is confined to solving for the first term in the pressure expansion, P_1 , while the velocity equations remain strictly hyperbolic. Given the solution for P_1 it is straightforward to use Eq. (41) to determine P_2 . This reduction in degrees of freedom reduces the complexity of the model and should contribute to increased overall computational efficiency.

3.3. Weakly nonlinear $O(\mu^N)$ solution

It is possible to extend the $O(\mu^2)$ solution to arbitrary order where all $O(\mu^N)$ terms are retained. However the extension of the fully nonlinear model to higher order leads to very complex equations and numerical implementation becomes difficult. For this reason we explore a weakly nonlinear model for arbitrary $N \geq 4$ where all terms of $O(\delta \mu^4)$ or greater are truncated, the implementation of the fully nonlinear model will be left to future work. Details of the general formula for the higher order solution can be found in Appendix A. As it is shown in Appendix A, a reduction in the degrees of freedom for the problem is possible. In general a

full reduction in degrees of freedom for a pressure expansion of order $O(\mu^N)$ will lead to a set of $N - 2$ elliptic equations to be solved.

4. Analytic properties

As with classical Boussinesq theory, the linear and nonlinear properties of the pressure-Poisson model can be assessed through linear and nonlinear expansions. Results show that the model converges to the well known Stoke's solution at high-order for linear properties. Increased accuracy can be achieved when arbitrary vertical basis functions for pressure are used and appropriate coefficients are chosen so as to optimize for linear and nonlinear properties. In this section, Stoke's type analysis and multiple scales analysis are performed to explore the linear and nonlinear properties of the model and to determine the set of basis functions leading to optimal performance of the model.

4.1. Linear dispersion

We consider the first order dispersion properties of a small amplitude wave train over a flatbed. The approximate dispersion relationship can then be compared with the well known Airy dispersion relationship (Dean and Dalrymple, 1991) given by $C_{Airy}^2/gkh = \tanh(kh)/(kh)$. Details of the derivation are standard and can be found in Appendix B. The order of accuracy for the approximate dispersion relationship is reliant on three important components of the model, (1) the order of approximation in the pressure solution N , (2) the choice of basis functions ϕ_n , Eq. (15), and (3) for the $N = 2$ case the choice of weighting functions, w_m , Eq. (21).

We begin with the simplest case, $N = 2$. We consider basis and weighting functions,

$$\phi_1 = 1 - q, \quad (43)$$

$$\phi_2 = \hat{\phi}_{12}(1 - q) + (1 - q^2), \quad (44)$$

$$w_1 = \widehat{W}_{01} + q, \quad (45)$$

which provides the following dispersion relationship,

$$\frac{C^2}{gh} = \frac{1 + B(kh)^2}{1 + (B + \frac{1}{3})(kh)^2}, \quad (46)$$

where,

$$B = -\frac{2 + \hat{\phi}_{12} + 4\widehat{W}_{01} + 3\hat{\phi}_{12}\widehat{W}_{01}}{12\widehat{W}_{01} + 6}. \quad (47)$$

Eq. (46) is equivalent to the general dispersion relationship derived by Madsen et al. (1991). As demonstrated by Madsen the appropriate choice of coefficients affects the accuracy of the dispersion relationship. If the basis functions and weighting functions are taken to be monomial, corresponding to a choice of $\hat{\phi}_{12} = 0$, $\widehat{W}_{01} = 0$ and $B = -\frac{1}{3}$, then the dispersion relationship becomes

$$\frac{C^2}{gh} = 1 - \frac{1}{3}(kh)^2, \quad (48)$$

which is equivalent to the dispersion relationship for the model derived by Nwogu (1993) expanded about the still water level, $z_x = 0$. This dispersion relationship has a formal accuracy of $O(\mu^2)$; however it produces a negative value for $kh > 3$, setting a limit on the applicability of the model, as a negative dispersion relationship will lead to imaginary celerity in the solution. As a result, the use of monomial basis and weighting functions is not recommended. It is noted here that if the pressure expansion is chosen to be given by Eq. (16) then the dispersion relationship for the

model is given by Eq. (48), regardless of choice of basis or weighting functions. It is for this reason that an expansion about the still water pressure, Eq. (18) was considered for the model.

An optimal choice of coefficients in the weighting function can produce a more accurate model. The optimal choice,

$$\hat{W}_{01} = -\frac{1}{3} \frac{5\hat{\phi}_{12} + 12}{5\hat{\phi}_{12} + 8}, \quad (49)$$

corresponding to $B = \frac{1}{15}$, produces the well known Padé [2,2] approximation to the Airy dispersion relationship,

$$\frac{C^2}{gh} = \frac{1 + \frac{1}{15}(kh)^2}{1 + \frac{2}{5}(kh)^2}, \quad (50)$$

which has a formal accuracy of $O(\mu^4)$. In addition, we still have one free parameter $\hat{\phi}_{12}$ which no longer affects the dispersion relationship, but as will be illustrated in the following section, will play a role in the accuracy of shoaling.

This technique can be extended to the $N = 4$ case with basis functions:

$$\phi_n = \sum_{m=1}^n \hat{\phi}_{mn}(1 - q^m), \quad \hat{\phi}_{nm} = 1, \quad n = 1 \dots 4, \quad (51)$$

$$W_n = \sum_{m=0}^n \widehat{W}_{mn} q^m, \quad \widehat{W}_{nn} = 1, \quad n = 1 \dots 3, \quad (52)$$

which in turn provides four independent free parameters, for simplicity we define

$$K_1 \equiv \hat{\phi}_{13}\hat{\phi}_{24} - \hat{\phi}_{23}\hat{\phi}_{14}, \quad (53)$$

$$K_2 \equiv \hat{\phi}_{13}\hat{\phi}_{34} - \hat{\phi}_{14}, \quad (54)$$

$$K_3 \equiv \hat{\phi}_{23}\hat{\phi}_{34} - \hat{\phi}_{24}, \quad (55)$$

$$K_4 \equiv \hat{\phi}_{13}. \quad (56)$$

The general dispersion relation then becomes,

$$\frac{C^2}{gh} = \frac{1 + A_1(kh)^2 + A_2(kh)^4 + A_3(kh)^6}{1 + A_4(kh)^2 + A_5(kh)^4}, \quad (57)$$

where

$$A_1 = \frac{1}{12}(2 - K_3 + 2K_4), \quad (58)$$

$$A_2 = \frac{1}{360}(-12 + 5K_1 + 15K_2 + 10K_3 + 10K_4), \quad (59)$$

$$A_3 = \frac{1}{8640}(-40K_1 - 45K_2 - 48K_4), \quad (60)$$

$$A_4 = \frac{1}{12}(6 - K_3 + 2K_4), \quad (61)$$

$$A_5 = \frac{1}{72}(K_1 + 3K_2 + 6K_4). \quad (62)$$

The four free parameters, $K_1 - K_4$, can be manipulated to improve the dispersion characteristics, both in the sense of order of accuracy, and in the sense of asymptotic behavior. A choice of $K_1 = -24/35 - 42/25K_4$, $K_2 = 64/105 - 64/25K_4$ and $K_3 = 2/3 + 2K_4$ gives the well known Padé [4,4] approximant to the dispersion relation,

$$\frac{C^2}{gh} = \frac{1 + \frac{1}{9}(kh)^2 + \frac{2}{945}(kh)^4}{1 + \frac{4}{9}(kh)^2 + \frac{1}{63}(kh)^4}, \quad (63)$$

which is accurate up to $O(\mu^8)$. In order to get the $O(\mu^{10})$ accurate Padé [6,4] approximant

$$\frac{C^2}{gh} = \frac{1 + \frac{19}{165}(kh)^2 + \frac{2}{1485}(kh)^4 - \frac{1}{155925}(kh)^6}{1 + \frac{74}{165}(kh)^2 + \frac{26}{1485}(kh)^4}, \quad (64)$$

a choice of $K_1 = -21776/28875 + 42/25K_4$, $K_2 = 6464/9625 - 64/25K_4$ and $K_3 = 34/55 + 2K_4$ is required. It is noted that for both optimized dispersion cases there is a free variable, K_4 . Just as with the $O(\mu^2)$ case this free-variable will be used to optimize either shoaling or nonlinear effects while retaining optimum dispersion properties. Both the Padé [4,4] and Padé [6,4] represent a significant improvement in accuracy for dispersion, however, the Padé [6,4] approximant approaches $-\infty$ in the limit which will lead to imaginary celerity. Therefore the set of basis functions that lead to the Padé [4,4] approximant are considered more advantageous. We note that the free coefficient $\hat{\phi}_{12}$ does not appear in the system, nor do any of the coefficients associated with the arbitrary weighting functions.

In general an optimum set of basis functions can be found to provide a Padé [N,N] or Padé [N+2,N] approximant solution to the dispersion for all $N \geq 4$, thus obtaining accuracy in the dispersion up to order $O(\mu^{2N})$ or $O(\mu^{2N+2})$ respectively. However the Padé [N+2,N] solution is not recommended due to the fact that it will always lead to negative celerity for large dimensionless wavenumbers.

Fig. 1 shows the ratio of the approximate dispersion for optimal basis functions. For the $N = 2$ case the optimal basis function solution is accurate to within 10% of the analytical dispersion up to the nominal intermediate water limit ($0 \leq kh \leq \pi$). For the $N = 4$ case the choice of optimal basis functions gives accurate dispersion to within 5% of the analytical dispersion up to the deep water limit ($0 \leq kh \leq 2\pi$), which is well within the proposed application range of this model.

4.2. Shoaling properties

Extension of the linear dispersion analysis to include a perturbation solution with a multiple scales expansion will generate an approximation to the linear shoaling gradient. We consider the case where the solution has two spatial scales, a slow and fast derivative, x and \mathbb{X} respectively. The slow derivative is assumed to vary at a rate proportional to a parameter $\varepsilon \ll 1$. In addition the bathymetry is considered to be slowly varying, i.e. $\nabla h = \varepsilon \frac{\partial h}{\partial \mathbb{X}}$. Details of the shoaling gradient analysis can be found in Appendix B. Solutions to the shoaling gradient can be compared with the well known solution derived by Madsen and Srensen (1993), given by,

$$\begin{aligned} \gamma_h &= \frac{h}{\bar{\eta}^{(0)}} \frac{\partial \bar{\eta}^{(0)}}{\partial \mathbb{X}} \left(\frac{\partial h}{\partial \mathbb{X}} \right)^{-1} \\ &= -\frac{2kh \sinh(2kh) + 2(kh)^2(1 - \cosh(2kh))}{(2kh + \sinh(2kh))^2}. \end{aligned} \quad (65)$$

An estimation of the error between the approximate shoaling gradient and the Stokes solution can be calculated using the cumulative shoaling error by integrating the difference between the analytic and approximate shoaling gradient from shallow to deep water following the formula used by Chen and Liu (1995),

$$\frac{A}{A_{st}} = \exp \left[\int_0^{kh} \frac{\gamma_h(kh') - \gamma_B(kh')}{kh'} d(kh') \right], \quad (66)$$

where γ_B is the approximate shoaling gradient and γ_h is the Stoke's solution. As stated previously in Section 4.1, after optimizing the basis functions for dispersion for the $O(\mu^2)$ and $O(\mu^4)$, one free-coefficient remained that could be used to optimize the shoaling gradient. After optimizing the dispersion to be equivalent to the Padé [2,2] approximant, the $O(\mu^2)$ shoaling gradient becomes

$$\gamma_h = \frac{1}{8} \frac{A_1(kh)^{10} + A_2(kh)^8 + A_3(kh)^6 + (kh)^4 + A_5(kh)^2 + A_6}{\hat{\phi}_{12}(2(kh)^4 + 10(kh)^2 + 75)^2}, \quad (67)$$

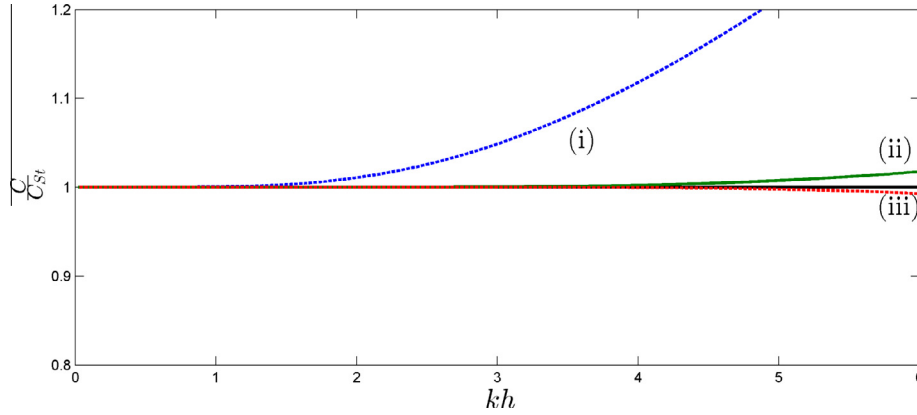


Fig. 1. Approximate linear dispersion relationships, C , compared with linear *Airy* dispersion, C_{st} , well past the nominal deep-water limit of $kh = \pi$; (i) optimum basis functions for $N = 2, O(\mu^4)$ Padé [2,2] accurate, (ii) optimum basis functions for $N = 4, O(\mu^8)$ Padé [4,4] accurate, and (iii) optimum basis functions $N = 4, O(\mu^{10})$ Padé [6,4] accurate.

where,

$$A_1 = 60\hat{\phi}_{12}^2 + 128\hat{\phi}_{12} + 64, \tag{68}$$

$$A_2 = 450\hat{\phi}_{12}^2 + 992\hat{\phi}_{12} + 480, \tag{69}$$

$$A_3 = 3000\hat{\phi}_{12}^2 + 6420\hat{\phi}_{12} + 3200, \tag{70}$$

$$A_4 = 5625\hat{\phi}_{12}^2 + 13200\hat{\phi}_{12} + 6000, \tag{71}$$

$$A_5 = 8250\hat{\phi}_{12}, \tag{72}$$

$$A_6 = -11250\hat{\phi}_{12}. \tag{73}$$

The approximate shoaling gradient, Eq. (67), has a Taylor expansion of,

$$\gamma_h = -\frac{1}{4} + \frac{1}{4}(kh)^2 + \left(\frac{1}{360} \frac{45\hat{\phi}_{12}^2 + 88\hat{\phi}_{12} + 48}{\hat{\phi}_{12}} \right) (kh)^4 + O(\mu^6), \tag{74}$$

as compared with the Taylor expansion for the exact solution, Eq. (67),

$$\gamma_h = -\frac{1}{4} + \frac{1}{4}(kh)^2 - \frac{1}{18}(kh)^4 - \frac{1}{540}(kh)^6 + O(\mu^8). \tag{75}$$

There are several choices of $\hat{\phi}_{12}$ which can optimize the shoaling gradient for different properties; (i) setting $\hat{\phi}_{12} = -6/5 \pm 2/15\sqrt{21} \approx -1.2 \pm 0.61$ will cause the solution to match the Taylor expansion up to $O(\mu^4)$, (ii) a choice of $\hat{\phi}_{12} \in (-4/3, -4/5)$ will cause the limit of the approximate shoaling gradient to be positive, indicating that waves traveling from deep water will decrease in amplitude as they enter shallow water, and (iii) A choice of $\hat{\phi}_{12} = -0.704720$ will minimize the cumulative error in the shoaling gradient, Eq. (66), up to the nominal deep water limit of $kh = \pi$. The details of these three cases can be found in Table 2.

Table 2

Cases of optimized basis functions for improved shoaling and Stoke’s second harmonic properties for the fully nonlinear $O(\mu^2)$ model. The case used for the numerical validation studies is designated in bold.

Case #	Coefficients	Dispersion	Shoaling	Nonlinear	Notes
(i)	$\hat{\phi}_{12} = -6/5 + 2/15\sqrt{15}, \hat{W}_{01} = 2/3 - \sqrt{5/3}$	Padé [2,2]	$O(\mu^4)$	$O(\mu^2)$	
(ii)	$\hat{\phi}_{12} = -4/3, \hat{W}_{01} = -4/3$	Padé [2,2]	$O(\mu^2)$	$O(\mu^2)$	Bounded Shoaling Limit
(iii)	$\hat{\phi}_{12} = -0.704720$ $\hat{W}_{01} = -0.631192$	Padé [2,2]	$O(\mu^2)$	$O(\mu^2)$	Minimized Shoaling Error over $kh \in [0, \pi]$
(iv)	$\hat{\phi}_{12} = -353/225$ $\hat{W}_{01} = -187/21$	Padé [2,2]	$O(\mu^2)$	$O(\mu^4)$	

An analysis of Eq. (67) demonstrates that setting $A_1 = 0$, corresponding to $\hat{\phi}_{12} = -4/3$ or $\hat{\phi}_{12} = -4/5$, will not only cause the limit to be positive but will also cause the deep water limit to be zero, which matches the deep water limit of the *Airy* solution. It is important to note that the choices of $\hat{\phi}_{12}$ for both case (i) and case (iii) are outside of the range for which the deep water limit of the shoaling gradient is positive, which can lead to stability issues. Thus these two cases are not recommended.

Fig. 2 shows the results a comparison of cases (i)–(iii) for the $O(\mu^2)$ case. Given that case (ii) represents a range of values, we take $\hat{\phi}_{12} = -4/3$ in order to take advantage of the agreement with the deep water limit. As can be seen from the figure both the optimization for the infinite limit (ii) and the Taylor expansion optimization (i) provide similar results in terms of accuracy, however the $\hat{\phi}_{12} = -4/3$ case also has better deep to shallow water properties. Thus it is recommended that when optimizing shoaling for the $O(\mu^2)$ case the choice of $\hat{\phi}_{12} = -4/3$ be used.

A similar analysis is conducted on the $O(\mu^4)$ case, although the approximate shoaling gradient is more complex. For simplicity the formula is not given here, however the properties will be discussed. After choosing basis functions such that the dispersion is optimized to a Padé [4,4] approximant, the Taylor expansion of the approximate shoaling gradient becomes

$$\gamma_h = -\frac{1}{4} + \frac{1}{4}(kh)^2 - \frac{1}{18}(kh)^4 - \frac{1}{151200} \left(\frac{22491\hat{\phi}_{13}^2 - 9555\hat{\phi}_{13} - 125}{21\hat{\phi}_{13} - 5} \right) (kh)^6 + O(\mu^8). \tag{76}$$

As with the $O(\mu^2)$ case it is possible to define basis functions such that certain properties of the shoaling gradient are optimized: (v) a choice of $\hat{\phi}_{13} = 35/102 \pm 5/714\sqrt{1245} = 0.343 \pm 0.247$ will cause the solution to be formally accurate up to $O(\mu^6)$; (vi) the deep water

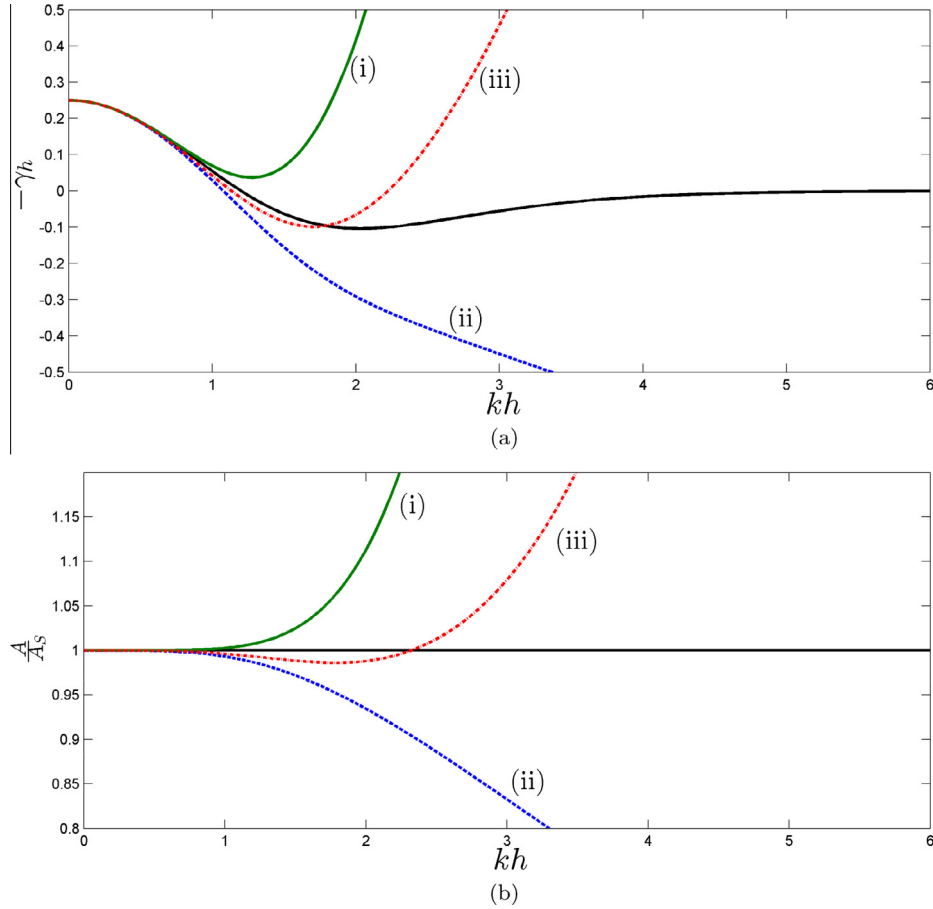


Fig. 2. Approximate shoaling gradient, γ_h , compared with linear theory well past the nominal deep-water limit shown for the $N = 2$ case, using optimum basis functions for cases (i)–(iii), see Table 2. The exact solution is shown as the solid black line. Direct comparison of shoaling gradients (top panel) and cumulative shoaling error (bottom panel).

limit of the shoaling gradient will be bounded with $\hat{\phi}_{13} = 10/19 \pm 10/399\sqrt{61} = 0.526 \pm 0.196$; and finally (vii) $\hat{\phi}_{13} = 0.60440$ will minimize the cumulative shoaling error, Eq. (66), over the interval $kh \in [0, \pi]$. The details of these three cases are shown in Table 3. We note that if $\hat{\phi}_{13} \in [0.3306, 0.7720]$ then the limit of the shoaling gradient will be positive, all three of the optimization cases shown here fall within these bounds. Fig. 3 shows a comparison between the Stoke's solution for the shoaling gradient and each of the three optimization cases. All three cases show good accuracy up to the nominal shallow water limit, with cases (v) and (vii) showing the closest agreement to the exact solution.

4.3. Nonlinear properties

A perturbation expansion of the dependent variables, $\eta = \eta^{(0)} + \varepsilon\eta^{(1)} + O(\varepsilon^2)$, is substituted into the model. First-order linear terms, $O(1, \delta)$, will match the first-order terms from the shoaling analysis and describe the dispersion properties of the model. The second-order linear terms combined with first-order nonlinear terms, $O(\varepsilon, \delta^2)$, will be different than those of the shoaling analysis and can be compared with the well known Stoke's second-order harmonic (Dean and Dalrymple, 1991). See Appendix C for details regarding the derivation of the second order harmonic term.

Recall that in the implementation, all models $O(\mu^4)$ or greater are weakly nonlinear. As a result all solutions for $N = 2$ will be formally fully nonlinear, while solutions for $N \geq 4$ will be weakly nonlinear. Fig. 4 shows a comparison of the ratios between the

approximate second harmonic, $\eta^{(1)}$ and the Stoke's second harmonic, η_{St} , for varying cases of optimized values. Details for each case can be found in Tables 2 and 3, for the $O(\mu^2)$ and $O(\mu^4)$ models respectively.

As with the case of shoaling, only one free-parameter, $\hat{\phi}_{12}$, is available at $O(\mu^2)$ to optimize nonlinear properties. Although there are several approaches to optimizing the nonlinear properties of the model, for brevity only one case is examined: (iv) choosing $\hat{\phi}_{12} = -353/225$ optimizes the nonlinear accuracy making the formal accuracy of the second harmonic $O(\mu^4)$. The top panel of Fig. 4 shows the ratios of the approximate solution and the Stoke's solution for the $O(\mu^2)$ implementation. The first three cases, (i)–(iii), represent the three optimized shoaling cases previously discussed. For these cases the formal accuracy of the approximate second harmonic is $O(\mu^2)$. As can be seen in the figure all four cases have reasonable accuracy for very shallow waves, but cases (i) and (iii) begin to diverge after $kh = 0.5$. Cases (ii) and (iv) are able to maintain good agreement with the analytical solution throughout the shallow water region. For all of these cases the dispersion has been optimized to a Padé [2,2] approximant.

For the $O(\mu^4)$ case there are two free-parameters that allow for the optimization of the solution. The first is $\hat{\phi}_{13}$, which can also be used to optimize shoaling, and the second is $\hat{\phi}_{12}$, which only appears in the equation for the nonlinear solution. For brevity, two possible approaches for optimizing the nonlinear properties are examined. We first consider the optimal shoaling cases (v)–(vii) with $\hat{\phi}_{12} = -2144/1197 - 8/1425\hat{\phi}_{13}$ chosen such that the second harmonic is formally accurate up to $O(\mu^4)$. Case

Table 3

Cases of optimized basis functions for improved shoaling and Stoke's second harmonic properties for the weakly nonlinear $O(\mu^4)$ model. The case used for the numerical validation studies is designated in bold.

Case #	Coefficients	Dispersion	Shoaling	Nonlinear	Notes
(v)	$\hat{\phi}_{12} = -60812/33915 \pm 4/101745\sqrt{1245}$ $\hat{\phi}_{13} = 35/102 \mp 5/714\sqrt{1245}$ $\hat{\phi}_{23} = (-41450 \mp 2229\sqrt{1245})/57210$ $\hat{\phi}_{14} = (2185 \pm 89\sqrt{1245})/3570$ $\hat{\phi}_{24} = (-118730 \mp 1429\sqrt{1245})/57120$ $\hat{\phi}_{34} = 1$	Padé [4,4]	$O(\mu^6)$	$O(\mu^4)$	
(vi)	$\hat{\phi}_{12} = -(204016 \pm 16\sqrt{61})/113715$ $\hat{\phi}_{13} = 10/19 \pm 10/399\sqrt{61}$ $\hat{\phi}_{23} = (29452 \mp 3153\sqrt{61})/15690$ $\hat{\phi}_{14} = 2(1261 \pm 89\sqrt{61})/1995$ $\hat{\phi}_{24} = (2012 \mp 3953\sqrt{61})/15960$ $\hat{\phi}_{34} = 1$	Padé [4,4]	$O(\mu^4)$	$O(\mu^4)$	Bounded Shoaling Limit
(vii)	$\hat{\phi}_{12} = -1.79454, \hat{\phi}_{13} = 0.60440$ $\hat{\phi}_{23} = 0.605257, \hat{\phi}_{14} = -1.54214$ $\hat{\phi}_{24} = -1.27021, \hat{\phi}_{34} = 1$	Padé [4,4]	$O(\mu^4)$	$O(\mu^4)$	Minimized Shoaling Error over $kh \in [0, \pi]$
(viii)	$\hat{\phi}_{12} = -0.1206296$ $\hat{\phi}_{13} = -1.790467$ $\hat{\phi}_{23} = 1.45195, \hat{\phi}_{14} = 6.98359$ $\hat{\phi}_{24} = 4.36622, \hat{\phi}_{34} = 1$	Padé [4,4]	$O(\mu^4)$	$O(\mu^4)$	Bounded Stoke's Limit
(ix)	$\hat{\phi}_{12} = -1.709480, \hat{\phi}_{13} = 0.60440$ $\hat{\phi}_{23} = 0.605257, \hat{\phi}_{14} = -1.54214$ $\hat{\phi}_{24} = -1.27021, \hat{\phi}_{34} = 1$	Padé [4,4]	$O(\mu^4)$	$O(\mu^2)$	Minimized Shoaling & Stoke's Error over $kh \in [0, \pi]$

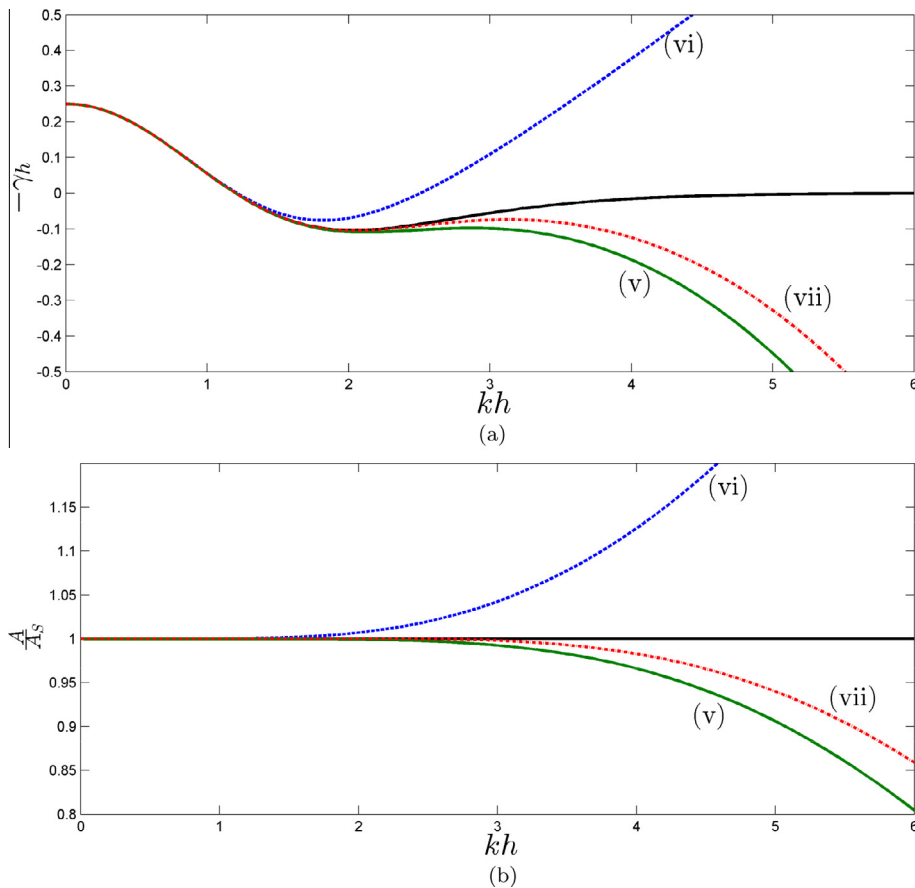


Fig. 3. Approximate shoaling gradient, γ_h , compared with linear theory well past the nominal deep-water limit shown for the $N = 4$ case, using optimum basis functions for cases (v)–(vii), see Table 3. Direct comparison of shoaling gradients (top panel) and cumulative shoaling error (bottom panel).

(viii) optimizes the nonlinear terms to $O(\mu^4)$ accuracy as well as makes the deep water limit close to zero with a choice of $\hat{\phi}_{31} = -1.790467$ and $\hat{\phi}_{12} = -0.1206296$. Lastly, case (ix)

minimizes the shoaling and nonlinear error over the nominal shallow water range, $kh \in [0, \pi]$ with a choice of $\hat{\phi}_{31} = 0.60440$ and $\hat{\phi}_{12} = -1.709480$.

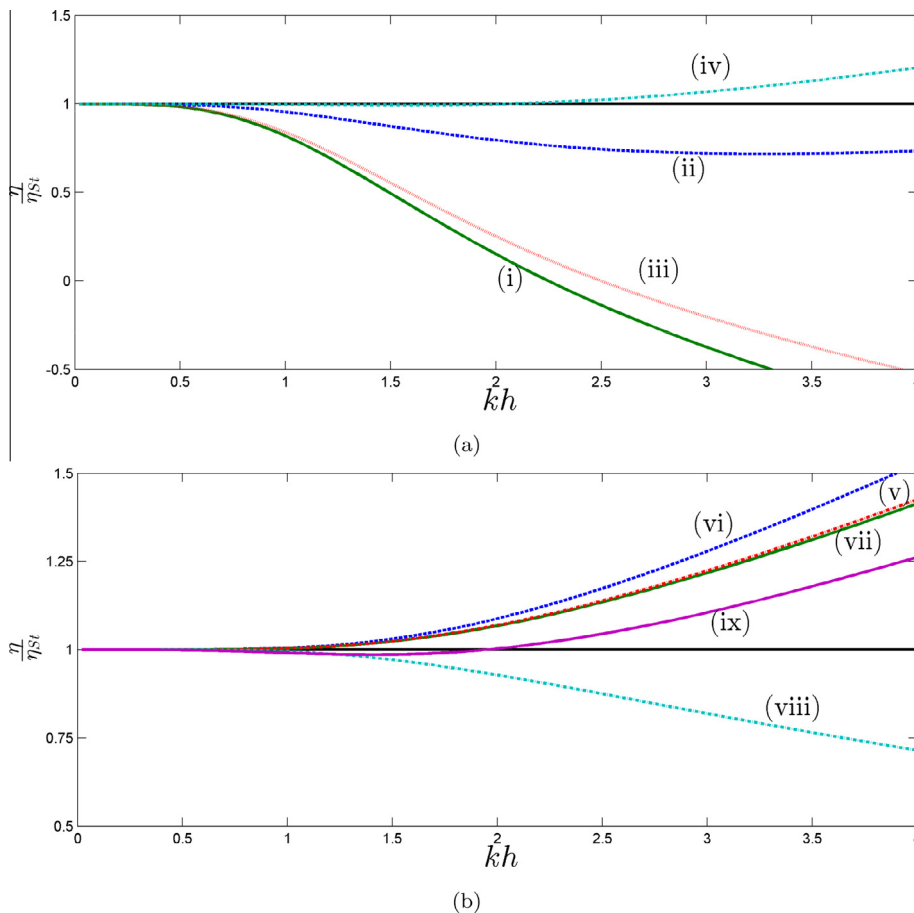


Fig. 4. Ratio of approximate second harmonic, η , to Stoke's second harmonic, η_{St} , for $N = 2$ case (top panel) and $N = 4$ case (bottom panel) using optimized dispersion, shoaling and nonlinearity, nonlinear cases (i)–(ix), see Tables 2 and 3.

The bottom panel of Fig. 4 show the ratios for the $O(\mu^4)$ implementation. Each of the five cases demonstrate good agreement with the Stoke's solution in the shallow water regime, with cases (viii) and (ix) showing the highest accuracy at the nominal shallow water limit. All five cases remained stable for the numerical validation cases and showed excellent agreement in comparison with experimental/analytical results. For brevity only the results of simulations from case (viii) are included in the validation section.

5. Numerical validation

5.1. Numerical algorithm and boundary condition treatment

Second-order central finite differences are used for the spatial derivatives and the time dependent hyperbolic component of the model is solved using a second order leap-frog scheme. Solutions to the pressure profile are found using a tri-diagonal solver for the elliptic problem for $O(\mu^2)$ and an LU solver for $O(\mu^4)$. In order to avoid the generation of high frequency spurious oscillations in the solution a one-dimensional Arakawa staggered C grid in space was used such that the pressure, P , and free-surface elevation, η , are defined at each node and the velocity, u , is defined at each half-node. Following the example of Zijlema et al. (2011) the temporal domain is also staggered such that the velocity solution is offset in time from the free-surface and pressure solution by half a time step. In all cases discussed in this section the boundary conditions are taken to be reflective.

In cases where the initial conditions involve the generation of waves, the generating-absorbing sponge layer technique developed

by Zhang et al. (2014) was used. The computational domain is broken up into three distinct sections. The first section represents a wave generation region of length L_1 , the second section is of length L_2 and represents a computational zone, the third section of length L_3 represents a wave absorption region where the incoming waves are gradually damped. Fig. 5(a) shows an example setup where the wave generation region is of length $L_1 = 5$, the computational area is of length $L_2 = 32$ and the wave absorption region is of length $L_3 = 10$.

5.2. Linear wave propagation

A simple case of the propagation of a small amplitude monochromatic wavetrain is examined. Waves of wavelength $L = 5h$, where h is the depth, are generated in the source region and allowed to propagate downstream. The spatial domain setup follows the diagram shown in Fig. 5(a). As seen in Fig. 5(b), the waves initially generated in the source region are accurately propagated downstream. Upon reaching the sponge layer region the wave-absorption is seen as the waves gradually decrease in amplitude until eventually reaching an amplitude of nearly zero. It should be noted that in this case the boundary conditions are treated as reflective. However, given the strength of the wave generation-absorption method, any reflections that occur at the boundaries are damped by the sponge layers.

5.3. Regular wave generation accuracy

In order to evaluate the accuracy of the wave generation-absorption a set of model runs were conducted for various degrees of non-

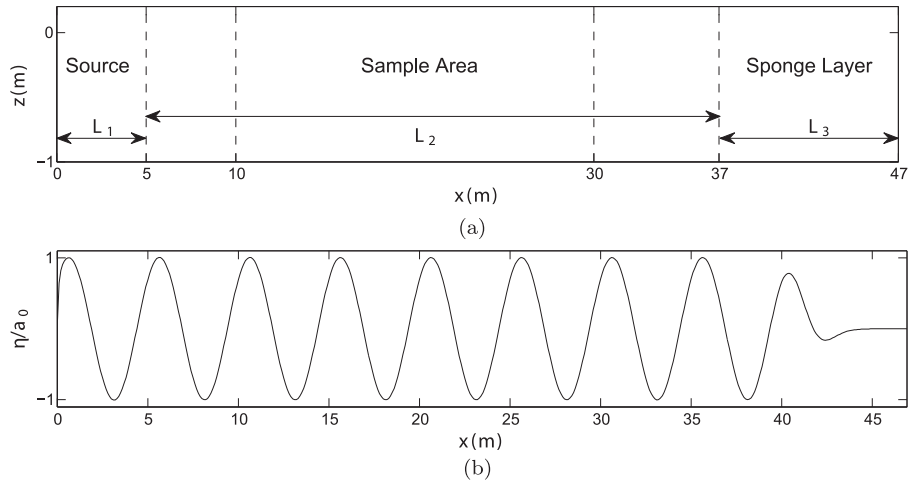


Fig. 5. Computational domain for sponge layer simulations (a) and an example of linear wave generation over this domain (b).

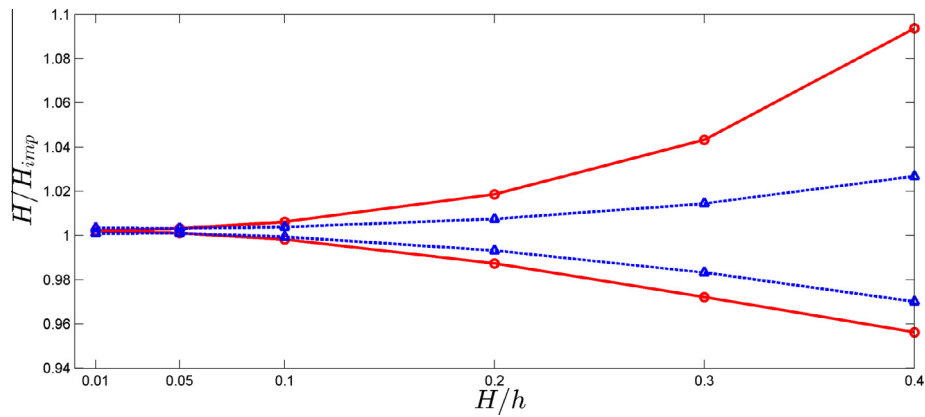


Fig. 6. Maximum and minimum wave heights recorded over a 20 m sample area for varying imposed wave heights, H_{imp} . Results are shown for the fully nonlinear $O(\mu^2)$ solution, solid red line with circles, and for the weakly nonlinear $O(\mu^4)$ solution, dashed blue line with triangles. (For interpretation of the references to colour in this figure caption, the reader is referred to the web version of this article.)

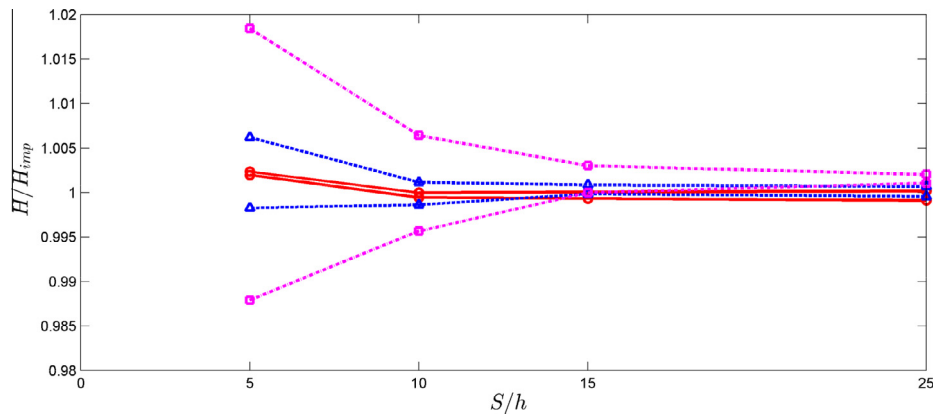
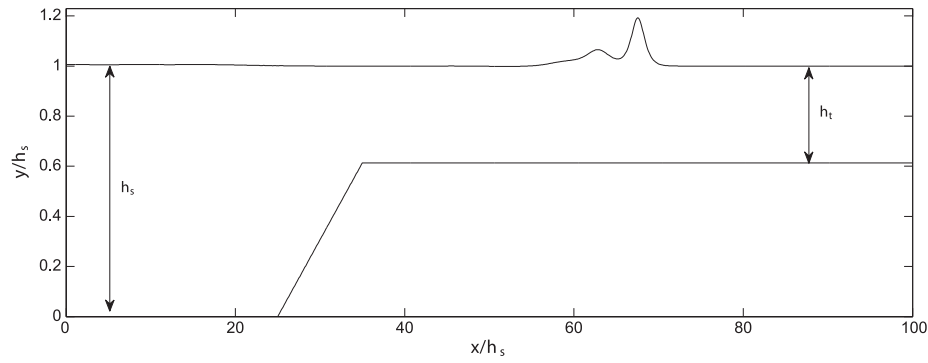


Fig. 7. Maximum and minimum wave heights recorded over a 20 m sample are for varying sponge lengths, S . All simulations shown were conducted using the fully nonlinear $O(\mu^2)$ model. Three imposed wave heights are shown, $H_{imp}/h = 0.01$: red solid line with circles, $H_{imp}/h = 0.1$: blue dashed line with triangles, and $H_{imp}/h = 0.2$: magenta dash-dot line with squares. (For interpretation of the references to colour in this figure caption, the reader is referred to the web version of this article.)

linearity. The model domain is the same as the test case described in Section 5.2. A wave of length $L = 5h$ is generated in a channel of depth h , corresponding to $kh = 1.25664$ and $T\sqrt{g/h} = 6.07898$. In all cases the integrated sponge strength is $\bar{\omega}_1 = 10\sqrt{gh}$ and the sponge is quadratically varying, see Zhang et al. (2014) for more details regarding

the sponge layer setup. The wavetrain is allowed to propagate for 15 wave periods before a record is made of the solution in a range of length $20h$ located at a distance of $5h$ from the edge of the wave generation region and $7h$ from the edge of the wave absorption region. At each spatial domain point the wave heights are averaged over five



(a) Bottom topography

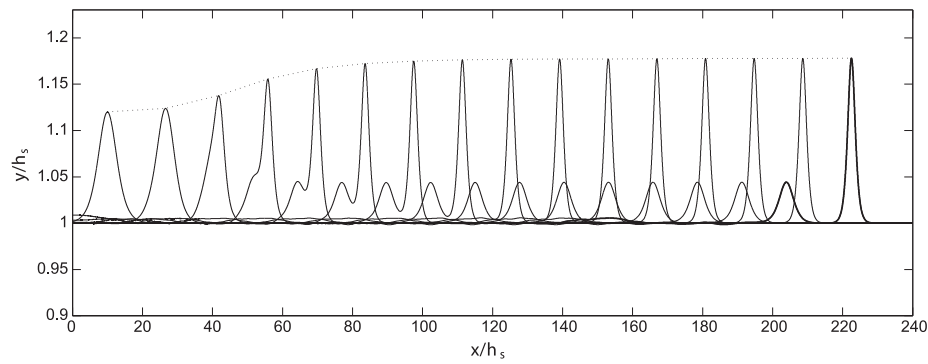
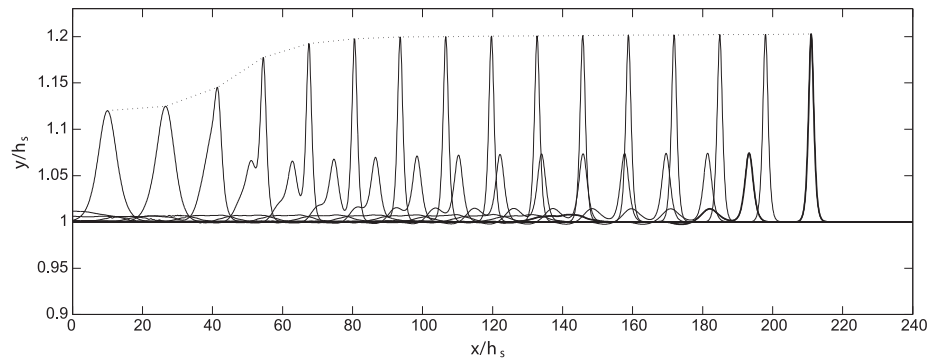
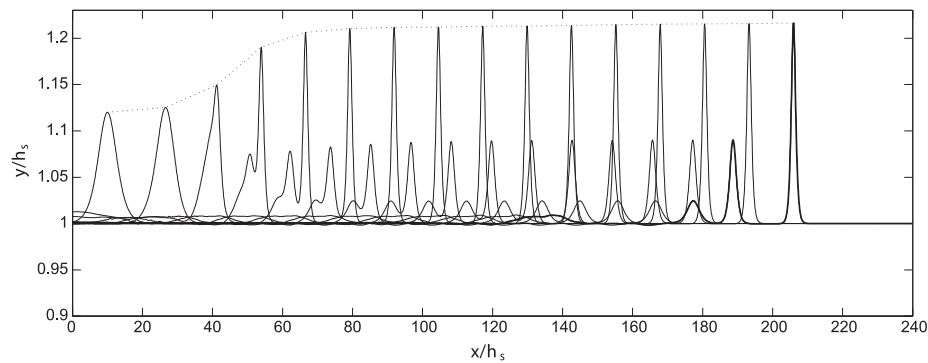
(b) $h_t/h_s = 0.6137$ (c) $h_t/h_s = 0.5$ (d) $h_t/h_s = 0.4510$

Fig. 8. Evolution of a solitary wave traveling over a shelf. The ratio of the solitary wave height to reference depth, h_s , is 0.12 in all cases. The final time solution is shown with a bold line, the dotted line designates the height of the leading soliton. Each of the three cases represent a different shelf height h_t .

wave periods. The maximum and minimum wave heights over the recorded region are then compared with the imposed wave height from the wave generation region. Fig. 6 shows the results of this analysis, for both the fully nonlinear $O(\mu^2)$ model, hereafter referred to as

the PP2 model, and the weakly nonlinear $O(\mu^4)$ model, hereafter referred to as the PP4 model.

The measured wave heights compare very well with the imposed wave heights for small amplitude waves. As the amplitude

Table 4

Comparison of wave height results for the case of a soliton propagating over shelves of different heights with an incident wave height of $H/h_s = 0.12$ where h_s is the depth of the channel prior to the shelf and h_t represents the height of the shelf.

H/h_s						
h_t/h_s	PP2	PP4	LPA ($n = 7$)	GN	KdV	Bouss.
0.6137	0.1779	0.1772	0.1745	0.168	0.181	–
0.5	0.2029	0.2010	0.1988	0.184	0.207	0.20
0.4510	0.2167	0.2137	0.2120	0.190	0.220	–

is increased, nonlinear effects become more prominent and the error in the measured wave heights increases. Given the higher order of accuracy inherent in the PP4 model, the error observed, even at strongly nonlinear waves, is relatively low. The imposed wave in the generation layer was of first order and we would expect the errors to increase at a quadratic rate and this is observed in these results.

It was found through the course of these tests that the size of the generation and absorption layer had an impact on the level of accuracy in the downstream propagated wave. Fig. 7 shows the results of testing sponge layers of different lengths, S , using the PP2 model. Three wave amplitudes were examined, a small wave amplitude, $H_{imp} = 0.01h$, serves as a reference, since it would be expected that such small amplitude waves would be accurately captured. It can be seen in the figure that for the smaller of the sponge lengths the small wave amplitude is accurately captured to within 0.5% and as the sponge length increases the solution approaches a steady solution that is very accurate. As the imposed wave amplitude is increased to $H_{imp} = 0.1h$ and $H_{imp} = 0.2h$ respectively a similar pattern is observed. The smaller sponge lengths are capable of capturing the solution to within 2% of the imposed amplitude, but as the sponge lengths are increased the accuracy of the solution increases to within 0.2%. A similar phenomenon was observed by Dommermuth (2000) for the gradual introduction of nonlinear interactions over time. Due to the nature of the sponge layer generation technique, the larger the sponge length the greater the distance over which the linear imposed wave dominates, allowing for a gradual introduction of the nonlinear interactions into the system.

Clear improvement for all three test cases is observed simply by increasing the length of the sponge layer from $S/h = 5$ to $S/h = 10$. In the case of an imposed wave height of $H_{imp} = 0.2$ the accuracy of the downstream wave improves from a maximum error of 1.8% to a maximum error of 0.6%, a similar observation is made for the minimum measured wave heights.

5.4. Propagation of a solitary wave over a shelf

As a first test of the model’s ability to predict nonlinear wave transformation, shoaling of a solitary wave is examined. The

domain is broken into three regions; an initial level of depth h_s and length $25h_s$, a plane slope of length $10h_s$ which reaches a shelf depth of h_t , and a final level of depth h_t and length $215h_s$. A solitary wave of height $0.12h_s$ propagates from the left hand boundary towards the shelf. Fig. 8(a) shows a schematic of the system. All numerical simulations were conducted with a spatial resolution of $\Delta x = 0.01$. A CFL number of 0.5 was chosen to maintain a low truncation error in the temporal solution while ensuring relatively good computational efficiency. The solution was allowed to propagate a sufficient amount of time to ensure that the leading soliton would reach a steady state near the right edge of the domain.

Johnson (1973) proved that according to KdV theory the solitary wave will break up into a finite number of solitons upon traveling over the shoal and that the number of solitons can be predicted by the ratio of the shelf depth to the initial depth, h_t/h_s . The results for the numerical model given three separate shelf depths are explored here; $h_t/h_s = 0.6137$, $h_t/h_s = 0.5$ and $h_t/h_s = 0.4510$. The first and third of these shelf depths are eigendepths of the KdV equation and according to theory the solitary wave should break up into two distinct solitons for the former case and three distinct solitons for the latter case. The second case was chosen to facilitate comparison with the Boussinesq-type solution of Madsen and Mei (1969). A time evolution of the results for each of the three cases is shown in Figs. 8(b)–8(d). In Fig. 8(b) at the final time step it is observed that the solitary wave has fissioned into two solitons that have propagated far downstream of the shelf, in agreement with the theory. Similarly, in Fig. 8(d) it is observed that the solitary wave breaks down into three solitons. It is noted that in all cases an oscillating wave is observed trailing the primary soliton train, this is a result of a deviation of the model from KdV theory. The amplitude of this wave is relatively small when compared with the amplitudes of the main soliton train.

Verification of the numerical results for both the PP2 model and the PP4 model is conducted through comparison of the leading soliton height with the heights predicted by KdV theory as well as the numerical results reported for the LPA model (Kennedy and Fenton, 1997). Green–Naghdi (GN) restricted Theory 1 Ertekin and Wehausen, 1986 and the previously mentioned numerical Boussinesq-type (Bouss.) solution (Madsen and Mei, 1969), these results can be found in Table 4. The Green–Naghdi, KdV and Boussinesq models reported here have a relatively low level of approximation and are not expected to perform as well when the waves become highly nonlinear. The LPA model has been demonstrated to be very accurate for cases of highly nonlinear waves and is considered to be the most accurate prediction for the purposes of comparison. Both the PP2 and PP4 results compare well with the LPA model, and as expected the higher order accuracy in the PP4 model provides results more closely aligned with the LPA results.

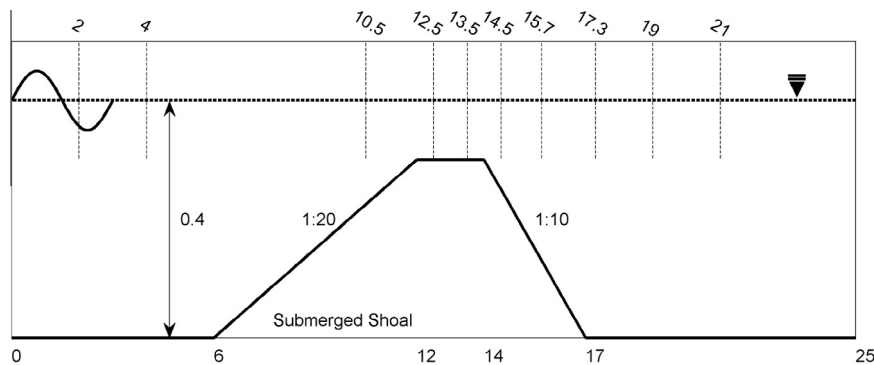


Fig. 9. Experimental setup for wave transformation over a submerged shoal, gauge locations are listed along the top axis, all units are in (m).

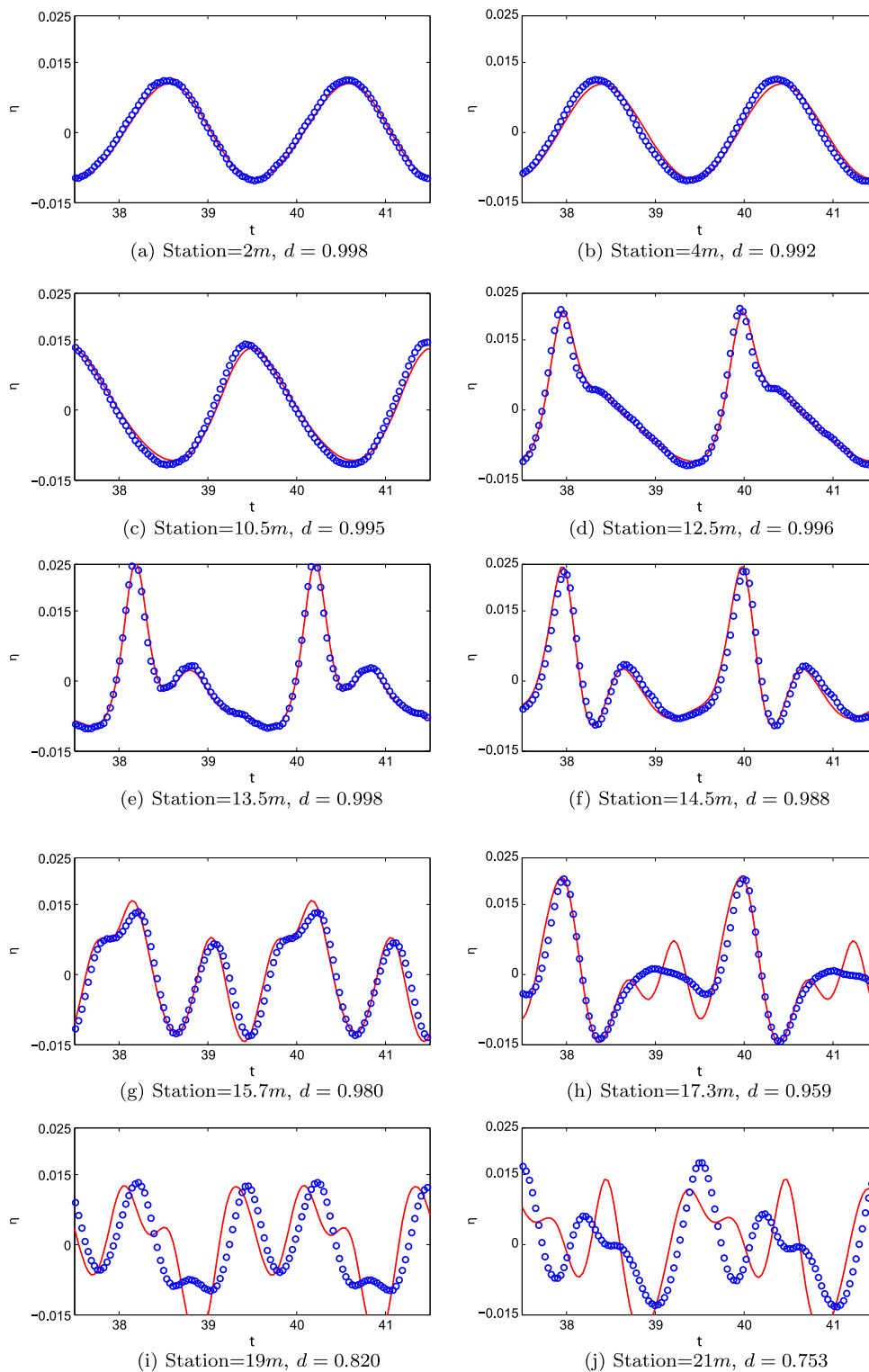


Fig. 10. Comparison for PP2 simulation on [Beji and Battjes \(1993\)](#) Case (A), between the observed data (circles) and modeled data (line), d represents the index of agreement, see Eq. (77). Numerical implementation using case (ii), see [Table 2](#).

5.5. Wavetrain traveling over a submerged shoal

The final validation of the model is conducted through comparison of numerical results with experimental results collected by [Beji and Battjes \(1993\)](#) on the effect of a wave train traveling over a submerged shoal. These experimental results have been used in many cases to validate a range of Boussinesq-type models

([Cienfuegos et al., 2007](#); [Gobbi and Kirby, 1999](#); [Roeber et al., 2010](#); [Yamazaki et al., 2009](#); [Zhang et al., 2013](#)). [Fig. 9](#) illustrates the experimental setup. A wave train is traveling from the left of the domain to the right in a channel of 0.4 m depth. The incoming wavetrain has a wave height of $H_0 = 0.020$ m and a wave period of $T = 2.02$ s, resulting in $kh = 0.67$. The upstream slope of the submerged shoal is 1:20 and begins 6 m into the domain, the down-

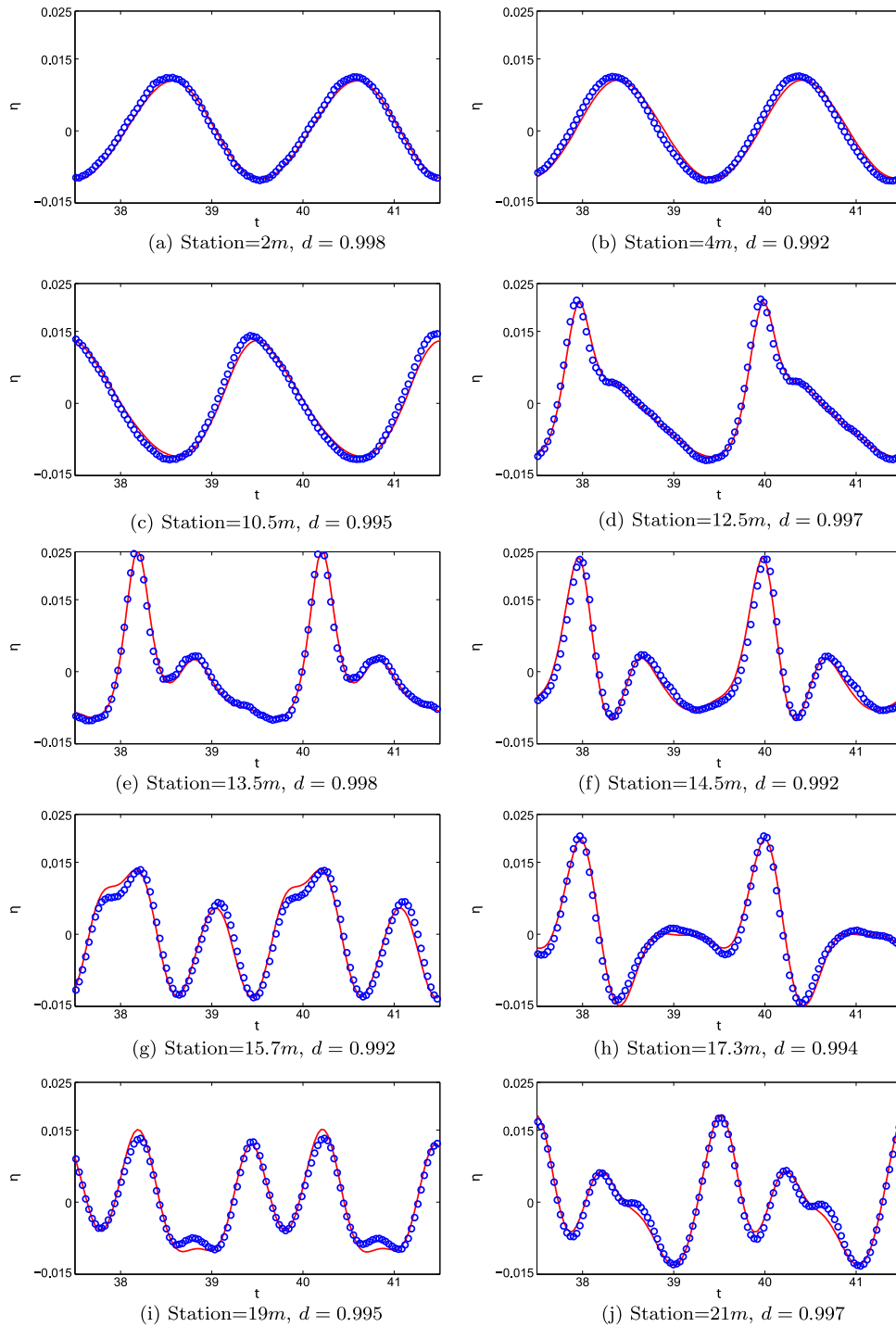


Fig. 11. Comparison for the PP4 simulation on *Beji and Battjes (1993) Case (A)*, between the observed data (circles) and modeled data (line), d represents the index of agreement, see Eq. (77). Numerical implementation using case (viii), see Table 3.

stream slope of the shoal is 1:10 and begins 14 m into the domain. The shoal has an overall height of 0.3 m and length of 11 m, see *Dingemans (1994)* for more details regarding the experimental setup. The experimental data set is composed of time histories for free-surface elevation at ten locations throughout the domain.

A quantitative assessment of the agreement between the model and the experimental results is conducted using the index of agreement, d , proposed by *Willmott (1981)* and later used by *Gobbi and Kirby (1999)* to assess the accuracy of WKGS, WN4 and FN4 models. The formula for d is as follows,

$$d = 1 - \frac{\sum_{j=n_1}^{n_2} [y(j) - y_d(j)]^2}{\sum_{j=n_1}^{n_2} [|y(j) - \bar{y}_d| + |y_d(j) - \bar{y}_d|]^2}, \quad (77)$$

where the points n_1 and n_2 are the bounds covering one full wave period, $y_d(j)$ represents measured data used for comparison, $y(j)$ represents predicted values from the model and \bar{y}_d is the average value of the observed data over one wave period. All simulations were conducted on a mesh spanning from -15 m to 30 m, with a grid spacing of $\Delta x = 0.025$ m and $\Delta t = 0.00025$ s. A small Δt value was chosen in order to facilitate a better match with the time history of the experimental data. Due to the sharp corners in

Table 5
Comparison of d values, see (77), between WKGS $O(\mu^2)$, FN4 $O(\mu^4)$ and WN4 $O(\mu^4)$ from Gobbi and Kirby (1999), Z2 $O(\mu^2)$ and Z4 $O(\mu^4)$ models from Zhang et al. (2013) and PP2 $O(\mu^2)$ and PP4 $O(\mu^4)$ solutions to the model for Beji and Battjes (1993) test case (A). $\Delta x = 0.025(m)$, $\Delta t = 0.0025(s)$, $x \in [-15, 30]$.

Gauge location (m)		PP2	WKGS	Z2	PP4	FN4	WN4	Z4
Upstream of the shoal	2	0.998	0.998	0.988	0.998	0.998	0.998	0.998
	4	0.992	0.996	0.973	0.992	0.996	0.996	0.998
	10.5	0.995	0.995	0.983	0.995	0.995	0.995	0.998
On the shoal	12.5	0.996	0.999	0.983	0.997	0.999	0.998	0.987
	13.5	0.998	0.996	0.986	0.998	0.995	0.987	0.980
	14.5	0.988	0.995	0.990	0.992	0.997	0.993	0.942
	15.7	0.980	0.995	0.992	0.992	0.996	0.980	0.967
Downstream of the shoal	17.3	0.994	0.975	0.972	0.994	0.995	0.972	0.977
	19	0.820	0.973	0.964	0.995	0.982	0.943	0.978
	21	0.753	0.927	0.902	0.997	0.993	0.962	0.976

the bathymetry, which cause discontinuities in the bathymetric derivatives, a five-point moving average filter was used with ten iterations. The smoothing was relatively minor at this grid scale and did not significantly alter the bathymetry.

Comparison of the numerical and experimental results are illustrated in Figs. 10 and 11 for the PP2 and PP4 models respectively. A comparison of the index of agreement is given in Table 5, along with the values reported by Gobbi and Kirby (1999) for the fully nonlinear $O(\mu^2)$ WKGS model and the two $O(\mu^4)$ models, WN4 (weakly nonlinear) and FN4 (fully nonlinear) and values for the fully nonlinear $O(\mu^2)$ and weakly nonlinear $O(\mu^4)$ fully rotational Green–Naghdi Boussinesq-type model developed by Zhang et al. (2013), Z2 and Z4 respectively.

Upstream of the shoal the wave propagation is relatively monochromatic and serves as a verification that the sponge layer wave generation boundary condition is producing the appropriate wave train, subfigures (a) and (b). As the wave train approaches the shoal the wave height begins to increase, a reflection of the shoaling dynamics. In addition the peaks become sharper indicating the separation of the wave energy into higher frequency waves, as seen in subfigures (c)–(e). Agreement between both the PP2 and PP4 models and the experimental data is very good in this region and on the same order as the models developed by Gobbi and Zhang. Once the wave train has passed over the shoal the dynamics of the problem become considerably more complex and the need for higher-order dispersion becomes more pronounced. The system now exhibits waves of many frequencies traveling at varying speeds, in addition the nonlinear interactions between the various wave frequencies becomes more prominent, as seen in subfigures (f)–(j). It is in this region that the benefit of added accuracy for dispersion, shoaling and nonlinear effects can be observed. The PP2 model does a poor job capturing the downstream solution, however the PP4 model does remarkably well. The index of agreement for stations downstream of the shoal for the PP4 model matches the fully nonlinear FN4 model and surpasses the weakly nonlinear WN4 and Z4 models.

6. Conclusions

The framework for a Boussinesq-type non-hydrostatic pressure model with a Green–Naghdi type expansion along the vertical axis has been developed. The resulting model is capable of resolving high-order dispersion, shoaling and nonlinear effects and when coupled with a SWE model produces a highly accurate solution for waves in both shallow and intermediate water. The vertical dimension in the model is handled through vertical modes in the pressure expansion, thus reducing the unknowns of the model to those resolving the horizontal dimensions. Through the application of asymptotic rearrangement, optimal vertical basis functions can be found which produce the highest order dispersion accuracy as

well as improved accuracy in the shoaling and nonlinear characteristics. The result is a relatively simple model to implement that is highly accurate.

In classical Boussinesq-type models the higher order dispersive terms are resolved through the inclusion of higher-order mixed space/time derivatives for the velocity. These mixed space/time derivatives can be difficult and inefficient to implement numerically. Similarly, extension of the model to two horizontal dimensions will involve mixed spatial derivatives, such as $\partial^3 u / (\partial x \partial y \partial t)$ and $\partial^3 v / (\partial x \partial y \partial t)$, which add an extra layer of computational complexity. While it is true that these issues have been largely addressed in the literature, in two horizontal dimensions there still remains a set of two elliptic equations to solve, one for each of the horizontal velocities, respectively. In contrast, the model developed in this work resolves the dispersive terms through the non-hydrostatic pressure component, which at $O(\mu^2)$ involves only a single equation to be solved, even for two-horizontal dimensions. Furthermore, the final forms of the model are simple and have fewer terms than many other comparable order equations.

The pressure–Poisson equation is a well known elliptic problem which does not exhibit mixed space/time derivatives or mixed spatial derivatives. Numerical implementation is straightforward and it is possible to take advantage of many of the well known techniques for solving elliptic problems. Through algebraic manipulation of the governing equations it is possible to reduce the degrees of freedom in the problem, which in turn will improve the computational efficiency of the model. A detailed comparison of the computational efficiency of the present model and the classic Boussinesq approach is outside the scope of this paper, however, research is currently under way to compare the present approach with other Boussinesq models. Analysis of computational cost and accuracy will be conducted.

The model was validated using a variety of test cases. It was demonstrated that the model is capable of capturing the relatively simple phenomenon of low amplitude wave propagation as well as the more complicated physics involved with a wavetrain traveling over a submerged shoal. In all test cases the numerical results of the model performed well in comparison to analytic and experimental data. In the case of the wavetrain traveling over a submerged shoal the results from the current model were compared with the results of the fully rotational Boussinesq model of Zhang et al. (2013), and the results computed by Gobbi and Kirby (1999), for fully nonlinear second-order models (Z2, WKGS) and weakly and fully nonlinear fourth-order models (Z4, WN4, FN4). The fully nonlinear second-order model demonstrated comparable performance with the models of Gobbi and Zhang in front of and upon the submerged shoal but showed decreased accuracy behind the shoal, demonstrating the need for higher order accuracy in the dispersive effects. However the current weakly nonlinear fourth order model was shown to be very accurate and to be comparable

in accuracy to the fully nonlinear fourth-order model of Gobbi (FN4) including the region behind the shoal.

The coupled pressure–Poisson/SWE model has been shown to be an accurate model for resolving the propagation of waves over variable bathymetry. Future work will focus on the implementation of breaking and wave runup in order to extend the realm of applicable problems to the model.

Acknowledgments

This work was funded under the National Science Foundation grant 1025519, and by the Office of Naval Research under the awards N00014-11-1-0045 and N00014-13-1-0123. Their support is gratefully acknowledged. Author Aaron S. Donahue was also partly supported by the Richard and Peggy Notebaert Fellowship program at the University of Notre Dame, author J.J. Westerink was also partly supported by the Henry J. Massman and the Joseph and Nona Ahearn endowments at the University of Notre Dame. The authors would also like to thank the anonymous reviewers whose comments and suggestions helped to improve this manuscript. Digital data files for wave propagation over a shoal were provided by Maarten Dingemans.

Appendix A. Weakly nonlinear $O(\mu^N)$ pressure problem

It is observed that solutions to the full set of equations follow a pattern. A pressure solution for an expansion of $O(\mu^N)$ can be found using the following expressions,

Bottom boundary condition:

$$\sum_{n=0}^N (a_{2,n} \cdot \nabla P_n + a_{1,n} P_n) = a_0 + O(\mu^{\beta_{N+2}}, \delta\mu^4), \quad (\text{A.1})$$

Pressure Poisson:

$$\sum_{n=0}^N (b_{3,n,m} \nabla \cdot \nabla P_n + b_{2,n,m} \cdot \nabla P_n + b_{1,n,m} P_n) = b_{0,m} + O(\mu^{\beta_{N+2}}, \delta\mu^4), \quad m = 1 \dots N-1, \quad (\text{A.2})$$

where,

$$a_{2,n} = \mu^{\beta_{n+2}} (h + \delta\eta) (\nabla h) \phi_n|_{q=0}, \quad (\text{A.3})$$

$$a_{1,n} = \left(\mu^{\beta_{n+2}} (\nabla h) \cdot (\nabla h) + \mu^{\beta_n} \right) \phi_n'|_{q=0}, \quad (\text{A.4})$$

$$a_0 = -\mathbf{g}(h + \delta\eta) + \delta\mu^2 (h + \delta\eta) \bar{\mathbf{u}} \cdot (\bar{\mathbf{u}} \cdot \nabla^2 h) \quad (\text{A.5})$$

and

$$b_{3,n,m} = \mu^{\beta_{n+2}} (h + \delta\eta)^2 \xi_{nm}|_{q=1}, \quad (\text{A.6})$$

$$b_{2,n,m} = 2\mu^{\beta_{n+2}} (h + \delta\eta) (\Theta_{nm} (\nabla h) - \Phi_{nm} (\nabla h + \nabla\eta))|_{q=1}, \quad (\text{A.7})$$

$$b_{1,n,m} = \mu^{\beta_n} \left[\left(\mu^2 (\nabla h)^2 + 1 \right) \Lambda_{nm} + \mu^2 S_{nm} ((\nabla h) + \delta(\nabla\eta))^2 - 2\mu^2 \Psi_{nm} (\nabla h) \cdot (\nabla h + \delta\nabla\eta) + \mu^2 \Theta_{nm} \left((h + \delta\eta) \nabla^2 h - 2\nabla h (\nabla h + \delta\nabla\eta) \right) + \mu^2 \Phi_{nm} \left(2(\nabla h + \delta\nabla\eta)^2 - (h + \delta\eta) (\nabla^2 h + \delta\nabla^2\eta) \right) \right] |_{q=1}, \quad (\text{A.8})$$

$$b_{0,m} = -\delta\mu^2 (h + \delta\eta)^2 \Omega_m \nabla (\bar{\mathbf{u}} \cdot \nabla \bar{\mathbf{u}})|_{q=1}, \quad (\text{A.9})$$

where,

$$\hat{\beta}_n = \begin{cases} 0 & \text{for } n = 0, \\ \beta_n & \text{otherwise} \end{cases} \quad (\text{A.10})$$

and the above integrals are defined in Table 1. It is important to note that, in order to construct a weakly nonlinear model, all terms that are of $O(\delta\mu^4)$ and higher are discarded in addition to all terms

that are of $O(\mu^{N+2})$. An advantage of considering the model in this framework is that all of the integrals as they are defined in Table 1 can be calculated once and substituted into the a_{ij} 's and b_{ijk} 's. A versatile algorithm can then be designed such that the elliptic solver is based on arbitrary a_{ij} 's and b_{ijk} 's.

The conservation of momentum equations follow a similar pattern and can be defined as,

$$\frac{\partial \bar{\mathbf{u}}}{\partial t} + \delta \bar{\mathbf{u}} \cdot \nabla \bar{\mathbf{u}} + \frac{1}{2} \mathbf{g} \left(\frac{h \nabla \eta + \eta \nabla h}{h + \delta\eta} \right) + \sum_{n=1}^N (C_{2,n} \nabla P_n + C_{1,n} P_n) = 0, \quad (\text{A.11})$$

where,

$$C_{2,n} = \mu^{\beta_n} G_n|_{q=1}, \quad (\text{A.12})$$

$$C_{1,n} = \mu^{\beta_n} \frac{-1}{h + \delta\eta} \left(\nabla h \phi_n|_{q=0} + \nabla h R_n|_{q=1} (\nabla h + \delta\nabla\eta) \right). \quad (\text{A.13})$$

Finally the conservation of mass equation remains unchanged,

$$\frac{\partial \eta}{\partial t} + \nabla \cdot ((h + \delta\eta) \bar{\mathbf{u}}) = 0. \quad (\text{A.14})$$

Eqs. (A.1), (A.2), (A.11) and (A.14) make up the complete system of equations for an arbitrary $O(\mu^N)$ model.

A.1. Reduction in degrees of freedom for higher order models

The technique for reducing the degrees of freedom in the fully nonlinear $O(\mu^2)$ case can be extended to the weakly nonlinear $O(\mu^N)$ case. Considering Eqs. (A.1) and (A.2), truncation of all terms of $O(\mu^{\beta_{N+2}})$ and nonlinear terms of order $O(\delta\mu^4)$ in the coefficients a_{ij} and b_{ijk} produces,

$$a_{1,N} P_N + \sum_{n=1}^{N-1} (a_{2,n} \cdot \nabla P_n + a_{1,n} P_n) = a_0 + O(\mu^{\beta_{N+2}}, \delta\mu^4), \quad (\text{A.15})$$

$$b_{1,N,m} P_N + \sum_{n=1}^{N-1} (b_{3,n,m} \nabla \cdot \nabla P_n + b_{2,n,m} \cdot \nabla P_n + b_{1,n,m} P_n) = b_{0,m} + O(\mu^{\beta_{N+2}}, \delta\mu^4), \quad m = 1 \dots N-1, \quad (\text{A.16})$$

where,

$$a_{1,N} = \mu^{\beta_N} \phi_N'|_{q=0} \in \mathbb{R}, \quad (\text{A.17})$$

$$b_{1,N,m} = \mu^{\beta_N} \Lambda_{Nm}|_{q=1} \in \mathbb{R}, \quad (\text{A.18})$$

which implies that P_N can be explicitly written in terms of the P_n for $n = 1 \dots N-1$, assuming $\phi_N'|_{q=0} \neq 0$. This reduces the number of unknowns in the elliptic equation by one and gives the following system of equations:

$$P_N = \frac{1}{a_{1,N}} \left(a_0 - \sum_{n=1}^{N-1} (a_{2,n} \cdot \nabla P_n + a_{1,n} P_n) \right), \quad (\text{A.19})$$

$$\sum_{n=1}^{N-1} (B_{3,n,m} \nabla \cdot \nabla P_n + B_{2,n,m} \cdot \nabla P_n + B_{1,n,m} P_n) = B_{0,m}, \quad m = 1 \dots N-1, \quad (\text{A.20})$$

where,

$$B_{3,n,m} = b_{3,n,m}, \quad (\text{A.21})$$

$$B_{2,n,m} = b_{2,n,m} - \left(\frac{b_{1,N,m}}{a_{1,N}} \right) a_{2,n}, \quad (\text{A.22})$$

$$B_{1,n,m} = b_{1,n,m} - \left(\frac{b_{1,N,m}}{a_{1,N}} \right) a_{1,n}, \quad (\text{A.23})$$

$$B_{0,m} = b_{0,m} - \left(\frac{b_{1,N,m}}{a_{1,N}} \right) a_0. \quad (\text{A.24})$$

Furthermore it is possible to reduce the elliptic problem by an additional degree of freedom due to the fact that for $N \geq 4$ any term of order $O(\mu^{\beta(N-1)+2})$ will also be truncated. For $m = 1$ Eq. (A.20) can be written as

$$B_{1,N-1,1}P_{N-1} + \sum_{n=1}^{N-2} (B_{3,n,1} \nabla \cdot \nabla P_n + B_{2,n,1} \cdot \nabla P_n + B_{1,n,1} P_n) = B_{0,1}, \quad (\text{A.25})$$

where,

$$B_{1,N-1,1} = \mu^{\beta N} \left(\Lambda_{(N-1)1} |_{q=1} - \Lambda_{N1} |_{q=1} \left(\frac{\phi'_{N-1}}{\phi'_N} \right)_{q=0} \right). \quad (\text{A.26})$$

This implies that P_{N-1} can be written as an explicit combination of the P_n terms for $n = 1 \dots N-2$, assuming that $B_{1,N-1,1} \neq 0$. Thus

$$P_N = \frac{1}{a_{1,N}} \left(a_0 - \sum_{n=1}^{N-1} (a_{2,n} \cdot \nabla P_n + a_{1,n} P_n) \right), \quad (\text{A.27})$$

$$P_{N-1} = \frac{1}{B_{1,N-1,1}} \left(B_{0,1} - \sum_{n=1}^{N-2} (B_{3,n,1} \nabla \cdot \nabla P_n + B_{2,n,1} \cdot \nabla P_n + B_{1,n,1} P_n) \right), \quad (\text{A.28})$$

$$\sum_{n=1}^{N-2} (\hat{B}_{3,n,m} \nabla \cdot \nabla P_n + \hat{B}_{2,n,m} \cdot \nabla P_n + \hat{B}_{1,n,m} P_n) = \hat{B}_{0,m}, \quad (\text{A.29})$$

$$m = 2 \dots N-1,$$

where,

$$\hat{B}_{3,n,m} = B_{3,n,m} - \left(\frac{B_{1,N-1,m}}{B_{1,N-1,1}} \right) B_{3,n,1}, \quad (\text{A.30})$$

$$\hat{B}_{2,n,m} = B_{2,n,m} - \left(\frac{B_{1,N-1,m}}{B_{1,N-1,1}} \right) B_{2,n,1}, \quad (\text{A.31})$$

$$\hat{B}_{1,n,m} = B_{1,n,m} - \left(\frac{B_{1,N-1,m}}{B_{1,N-1,1}} \right) B_{1,n,1}, \quad (\text{A.32})$$

$$\hat{B}_{0,m} = B_{0,m} - \left(\frac{B_{1,N-1,m}}{B_{1,N-1,1}} \right) B_{0,1}. \quad (\text{A.33})$$

No more reduction of degrees of freedom is possible in this manner. However this technique has reduced the degrees of freedom in the elliptic problem by two and in general the inclusion of an $O(\mu^N)$ pressure profile will lead to an additional $N-2$ elliptic equations to be solved. This reduction in the degrees of freedom will improve the computational cost of the method in the numerical implementation. For example, in one horizontal dimension the $O(\mu^4)$ model has only six bands in the elliptic problem using a central difference method. Note that the set of basis functions and weighting functions is arbitrary, thus the set of constant coefficients in each of these sets can be chosen in order to enforce $a_{1,N} \neq 0$ and $B_{1,N-1,1} \neq 0$, making the reduction in the degrees of freedom always possible.

Appendix B. Linear properties

In order to explore the dispersive and shoaling properties of the model we consider the linear case, i.e. $O(1)$, with a multiple scales expansion of the dependent variables. The multiple scales expansion consists of the case where spatially there is a fast derivative, x , and a slow derivative, \times , and we consider only one scale in the time domain, t . In addition we also consider that the bathymetry is slowly varying, i.e. $h_x = \varepsilon h_{\times}$, where $\varepsilon \ll 1$. Spatial derivatives to both pressure and free-surface are thus given by the following expressions:

$$P_{n,x} \rightarrow P_{n,x} + \varepsilon P_{n,\times} + O(\varepsilon^2), \quad (\text{B.1})$$

$$P_{n,xx} \rightarrow P_{n,xx} + \varepsilon (P_{n,\times\times} + P_{n,\times x}) + O(\varepsilon^2) \quad (\text{B.2})$$

and similar expressions for the free-surface spatial derivatives, η_x and $\eta_{\times x}$. Next we consider a perturbation solution to the dependent variables:

$$P_n = P_n^{(0)} + \varepsilon P_n^{(1)} + O(\varepsilon^2), \quad (\text{B.3})$$

$$\eta = \eta^{(0)} + \varepsilon \eta^{(1)} + O(\varepsilon^2), \quad (\text{B.4})$$

$$u_0 = u_0^{(0)} + \varepsilon u_0^{(1)} + O(\varepsilon^2). \quad (\text{B.5})$$

Substituting the multiples scales expansion and perturbation expansion, Eqs. B.1,B.2,C.10,C.11,B.5, into the governing equations and retaining only terms up to $O(\varepsilon, 1)$ we get the following set of equations:

$O(1, 1)$:

$$g\eta^{(0)} + \sum_{n=1}^N \mu^{\beta n} \phi_{n,q} |_{q=0} P_n^{(0)} = 0, \quad (\text{B.6})$$

$$\left[\mu^2 g h^2 \chi_m \eta_{,xx}^{(0)} + \sum_{n=1}^N \mu^{\beta n} (\mu^2 h^2 \zeta_{nm} P_{n,xx}^{(0)} + \Lambda_{nm} P_n^{(0)}) \right]_{q=1} = 0, \quad (\text{B.7})$$

$$m = 1 \dots N-1,$$

$$\eta_{,t}^{(0)} + h u_{0,x}^{(0)} = 0, \quad (\text{B.8})$$

$$h u_{0,t}^{(0)} + \frac{1}{2} g h \eta_{,x}^{(0)} + h \sum_{n=1}^N \mu^{\beta n} G_n |_{q=1} P_{n,x}^{(0)} = 0. \quad (\text{B.9})$$

$O(\varepsilon, 1)$:

$$g\eta^{(1)} + \sum_{n=1}^N \mu^{\beta n} \phi_{n,q} |_{q=0} P_n^{(1)} = - \sum_{n=1}^N \mu^{\beta n+2} h h_{,\times} \phi_n |_{q=0} P_{n,x}^{(0)}, \quad (\text{B.10})$$

$$\left[\mu^2 g h^2 \chi_m \eta_{,xx}^{(1)} + \sum_{n=1}^N \mu^{\beta n} (\mu^2 h^2 \zeta_{nm} P_{n,xx}^{(1)} + \Lambda_{nm} P_n^{(1)}) = 2\mu^2 g h h_{,\times} (\chi_m - \Omega_m) \eta_{,x}^{(0)} - \mu^2 g h^2 \chi_m (\eta_{,x\times}^{(0)} + \eta_{,\times x}^{(0)}) - \sum_{n=1}^N \mu^{\beta n} (\mu^2 h^2 \zeta_{nm} (P_{n,\times\times}^{(0)} + P_{n,\times x}^{(0)}) + 2\mu^2 h h_{,\times} (\Theta_{nm} - \Psi_{nm}) P_{n,x}^{(0)}) \right]_{q=1}, \quad (\text{B.11})$$

$$m = 1 \dots N-1,$$

$$\eta_{,t}^{(1)} + h u_{0,x}^{(1)} = -h_{,\times} u_0^{(0)} - h u_{0,\times}^{(0)}, \quad (\text{B.12})$$

$$h u_{0,t}^{(1)} + \frac{1}{2} g h \eta_{,x}^{(1)} + h \sum_{n=1}^N \mu^{\beta n} G_n |_{q=1} P_{n,x}^{(1)} = -\frac{1}{2} g h \eta_{,\times}^{(0)} - \frac{1}{2} g h_{,\times} \eta^{(0)} - \sum_{n=1}^N \mu^{\beta n} (h G_n P_{n,\times}^{(0)} + h_{,\times} (\phi_n - R_n) P_n^{(0)})_{q=1}, \quad (\text{B.13})$$

where the formulas for the above integrals can be found in Table 1. A general solution to the $O(1, 1)$ equations will provide an understanding of the linear dispersion properties, while a general solution to the $O(\varepsilon, 1)$ equations will lead to an analysis of the linear shoaling properties of the model. We apply the following general solutions to the above equations:

$$\eta^{(0)} = \tilde{\eta}^{(0)} e^{i\psi}, \quad P_n^{(0,1)} = \tilde{P}_n^{(0,1)} e^{i\psi}, \quad u_0^{(0,1)} = \tilde{u}_0^{(0,1)} e^{i\psi}, \quad (\text{B.14})$$

where $\eta^{(1)}$ is taken to be zero, i is the imaginary constant and $\psi = \psi(x, t)$ such that ψ is a periodic function in both x and t with frequency k and σ respectively, such that,

$$\eta_t^{(0)} = -i\sigma \tilde{\eta}^{(0)} e^{i\psi}, \quad \eta_x^{(0)} = ik \tilde{\eta}^{(0)} e^{i\psi}, \quad \eta_{xx}^{(0)} = -k^2 \tilde{\eta}^{(0)} e^{i\psi},$$

$$\eta_{,\times}^{(0)} = \tilde{\eta}_{,\times}^{(0)} e^{i\psi}, \quad \eta_{,\times x}^{(0)} = ik \tilde{\eta}_{,\times}^{(0)} e^{i\psi}, \quad \eta_{,\times \times}^{(0)} = ik_{,\times} \tilde{\eta}^{(0)} e^{i\psi} + ik \tilde{\eta}_{,\times}^{(0)} e^{i\psi},$$

and the same for $P_n^{(0,1)}$ and $u_0^{(0,1)}$. Furthermore, to simplify the solutions we define $\tilde{P}_n^{(0,1)}$ and $\tilde{u}_0^{(0,1)}$ in terms of transition functions $T_n(kh)^{(0,1)}$ and $S_0(kh)^{(0,1)}$ which are dependent on the depth h and the wavenumber k ,

$$\tilde{P}_n^{(0)} = g \tilde{\eta}^{(0)} T_n^{(0)}, \quad \tilde{u}_0^{(0)} = \sigma \tilde{\eta}^{(0)} S_0^{(0)},$$

$$\tilde{P}_n^{(1)} = i g h_{,\times} \tilde{\eta}^{(0)} T_n^{(1)}, \quad \tilde{u}_0^{(1)} = i h_{,\times} \sigma \tilde{\eta}^{(0)} S_0^{(1)}.$$

Considering that the shoaling coefficient, $\gamma_h = (h\tilde{\eta}'_x)/(h_x\tilde{\eta}^{(0)})$, is a function of the change in the free-surface with respects to the change in the bathymetry, we rewrite the slow derivative of η in terms of the shoaling coefficient γ_h , Eq. (65). Lastly we define a variable Q related to the dispersion relationship.

$$\tilde{\eta}'_{x,\times} = \left(\frac{h_{,\times}}{h}\right)\tilde{\eta}^{(0)}\gamma_h, \quad Q \equiv \frac{\sigma^2}{gh}.$$

From these it is also possible to derive the following relationships:

$$\begin{aligned} \widehat{Q} &= \frac{khQ_{,kh}}{Q + khQ_{,kh}}, \\ k_{,\times} &= -h_{,\times}\left(\frac{k}{h}\right)\widehat{Q}, \\ (kh)_{,\times} &= kh_{,\times}(1 - \widehat{Q}), \\ \tilde{P}'_{n,\times} &= g\left(\tilde{\eta}'_{n,\times}T_n^{(0)} + kh_{,\times}(1 - \widehat{Q})\tilde{\eta}^{(0)}T'_{n,kh}{}^{(0)}\right), \\ \tilde{u}'_{0,\times} &= \sigma\left(\tilde{\eta}'_{n,\times}S_0^{(0)} + kh_{,\times}(1 - \widehat{Q})\tilde{\eta}^{(0)}S'_{0,kh}{}^{(0)}\right). \end{aligned}$$

Substituting these relationships into Eqs. (B.6)–(B.13) we obtain the following system of equations:

$O(1, 1)$:

$$\sum_{n=1}^N \mu^{\hat{\beta}_n} \phi'_{n,q=0} T_n^{(0)} = -1, \quad (\text{B.15})$$

$$\left(\sum_{n=1}^N \mu^{\hat{\beta}_n} \left(\mu^2 (kh)^2 \xi_{nm} - \Lambda_{nm}\right) T_n^{(0)}\right)_{q=1} = 0, \quad (\text{B.16})$$

$$m = 1 \dots N - 1, \quad (\text{B.17})$$

$$\begin{aligned} S_0^{(0)} &= \frac{1}{kh}, \\ \frac{\sigma^2}{gk^2 h} &= \frac{C^2}{gh} = \frac{1}{2} + \sum_{n=1}^N \mu^{\hat{\beta}_n} G_n|_{q=1} T_n^{(0)}. \end{aligned} \quad (\text{B.18})$$

$O(\varepsilon, 1)$:

$$\sum_{n=1}^N \mu^{\hat{\beta}_n} \phi'_{n,q=0} T_n^{(1)} = -(kh) \sum_{n=1}^N \mu^{\hat{\beta}_n+2} \phi_{n,q=0} T_n^{(0)}, \quad (\text{B.19})$$

$$\begin{aligned} &\left[-2(kh)\mu^2 \left(\chi_m + \sum_{n=1}^N \mu^{\hat{\beta}_n} \xi_{nm} T_n^{(0)}\right) \gamma_h \right. \\ &\quad \left. + \sum_{n=1}^N \mu^{\hat{\beta}_n} \left(\mu^2 (kh)^2 \xi_{nm} - \Lambda_{nm}\right) T_n^{(1)}\right]_{q=1}, \\ &= \mu^2 (kh) (2\Omega_m - \chi_m (2 + \widehat{Q})) + \sum_{n=1}^N \mu^{\hat{\beta}_n+2} ((2(kh)(\Theta_{nm} - \Psi_{nm}) \\ &\quad - (kh)\widehat{Q}\xi_{nm}) T_n^{(0)} + 2(kh)^2 (1 - \widehat{Q})\xi_{nm} T'_{n,kh}{}^{(0)}) \Big]_{q=1}, \\ &m = 1 \dots N - 1, \end{aligned} \quad (\text{B.20})$$

$$S_0^{(0)} \gamma_h - (kh) S_0^{(1)} = (kh) (\widehat{Q} - 1) S_{0,kh}^{(0)} - S_0^{(0)}, \quad (\text{B.21})$$

$$\begin{aligned} &\left(\frac{1}{2} + \sum_{n=1}^N \mu^{\hat{\beta}_n} G_n T_n^{(0)}\right)_{q=1} \gamma_h + (kh)^2 \left(\frac{C^2}{gh}\right) S_0^{(1)} \\ &- (kh) \sum_{n=1}^N \mu^{\hat{\beta}_n} G_n|_{q=1} T_n^{(1)} = -\frac{1}{2} - \int_0^1 \sum_{n=1}^N \mu^{\hat{\beta}_n} \left((\phi_n - R_n) T_n^{(0)}\right. \\ &\quad \left. - (kh)(\widehat{Q} - 1) G_n T'_{n,kh}{}^{(0)}\right)_{q=1}. \end{aligned} \quad (\text{B.22})$$

The first-order pressure solutions can be found by solving Eqs. (B.15) and (B.16). From Eq. (B.18) it is clear that the dispersion relationship is directly related to the solution for the first order pressure terms, $T_n^{(0)}$. Once the $O(1, 1)$ solutions are found they can

be substituted into the $O(\varepsilon, 1)$ equations, (B.19)–(B.22) creating a system of equations. Solving this system of equations provides a solution for the shoaling gradient γ_h which can then be compared with the Stoke's solution for the shoaling gradient.

Appendix C. Nonlinear properties

In order to explore the nonlinear properties of the model we consider the nonlinear case, i.e. $O(\delta)$, with a flat bathymetry. As with the linear properties we consider a perturbation solution to the dependent variables:

$$P_n = P_n^{(0)} + \varepsilon P_n^{(1)} + O(\varepsilon^2), \quad (\text{C.1})$$

$$\eta = \eta^{(0)} + \varepsilon \eta^{(1)} + O(\varepsilon^2), \quad (\text{C.2})$$

$$u_0 = u_0^{(0)} + \varepsilon u_0^{(1)} + O(\varepsilon^2). \quad (\text{C.3})$$

Substituting the perturbation expansion into the governing equations and focusing on the $O(\varepsilon, \delta)$ terms we get the following set of equations:

$$g\eta^{(1)} + \sum_{n=1}^N \mu^{\hat{\beta}_n} \phi_{n,q} |_{q=0} P_n^{(1)} = 0, \quad (\text{C.4})$$

$$\begin{aligned} &g\mu^2 \chi_m |_{q=1} h^2 \eta_{,xx}^{(1)} + \sum_{n=1}^N \mu^{\hat{\beta}_n} \left(\mu^2 h^2 \xi_{nm} P_{n,xx} + \Lambda_{nm} P_n\right) |_{q=1} \\ &= -2\mu^2 h^2 \Omega_m |_{q=1} \left(u_x^{(0)}\right)^2 + gh\mu^2 \chi_m |_{q=1} \left(2(\eta_x^{(0)})^2 - \eta^{(0)} \eta_{,xx}^{(0)}\right) \\ &\quad - \sum_{n=1}^N \mu^{\hat{\beta}_n} \left(2\mu^2 \xi_{nm} \eta^{(0)} P_{n,xx}^{(0)} - 2\mu^2 h \Phi_{nm} (\eta_x^{(0)} P_{n,x}^{(0)} + \eta_{,xx}^{(0)} P_n^{(0)})\right) |_{q=1}, \\ &m = 1 \dots N - 1 \end{aligned} \quad (\text{C.5})$$

$$\eta_{,t}^{(1)} + hu_x^{(1)} = -\left(\eta_x^{(0)} u^{(0)} + \eta^{(0)} u_x^{(0)}\right), \quad (\text{C.6})$$

$$\begin{aligned} &\frac{1}{2} gh \eta_{,x}^{(1)} + hu_{,t}^{(1)} + \sum_{n=1}^N \mu^{\hat{\beta}_n} h G_n |_{q=1} P_{n,x}^{(1)} = -\eta^{(0)} u_{,t}^{(0)} - h \eta^{(0)} u_x^{(0)} \\ &\quad + \sum_{n=1}^N \mu^{\hat{\beta}_n} \left(R_n \eta_x^{(0)} P_n^{(0)} - G_n \eta^{(0)} P_{n,x}^{(0)}\right) |_{q=1}. \end{aligned} \quad (\text{C.7})$$

Note that the $O(1)$ equations are equivalent to the $O(1)$ equations from Appendix B. A general solution to the above equations will lead to an approximation for the nonlinear properties of the model. We apply the following general solutions,

$$\eta^{(0)} = \tilde{\eta}^{(0)} e^{i\psi}, \quad P_n^{(0,1)} = \tilde{P}_n^{(0,1)} e^{i\psi}, \quad u_0^{(0,1)} = \tilde{u}_0^{(0,1)} e^{i\psi}, \quad (\text{C.8})$$

where i is the imaginary constant and $\psi = \psi(x, t)$ such that ψ is a periodic function in both x and t with frequency k and σ respectively, such that,

$$\begin{aligned} \eta_{,t}^{(0)} &= -i\sigma \tilde{\eta}^{(0)} e^{i\psi}, & \eta_x^{(0)} &= ik \tilde{\eta}^{(0)} e^{i\psi}, & \eta_{,xx}^{(0)} &= -k^2 \tilde{\eta}^{(0)} e^{i\psi}, \\ \eta_{,t}^{(1)} &= -2i\sigma \tilde{\eta}^{(0)} e^{i\psi}, & \eta_x^{(1)} &= 2ik \tilde{\eta}^{(0)} e^{i\psi}, & \eta_{,xx}^{(1)} &= -4k^2 \tilde{\eta}^{(0)} e^{i\psi}. \end{aligned}$$

and the same for $P_n^{(0,1)}$ and $u_0^{(0,1)}$. Furthermore, to simplify the solutions we define $\tilde{P}_n^{(0,1)}$ and $\tilde{u}_0^{(0,1)}$ in terms of transition functions $T_n(kh)^{(0,1)}$ and $S_0(kh)^{(0,1)}$ which are dependent on the depth h and the wavenumber k , and define $\tilde{\eta}^{(1)}$ in terms of the first order wave height $\tilde{\eta}^{(0)}$,

$$\begin{aligned} \tilde{\eta}^{(1)} &= \tilde{A}(\tilde{\eta}^{(0)})^2, \\ \tilde{P}_n^{(0)} &= g\tilde{\eta}^{(0)} T_n^{(0)}, & \tilde{u}_0^{(0)} &= \sigma \tilde{\eta}^{(0)} S_0^{(0)}, \\ \tilde{P}_n^{(1)} &= ig(\tilde{\eta}^{(0)})^2 T_n^{(1)}, & \tilde{u}_0^{(1)} &= i\sigma(\tilde{\eta}^{(0)})^2 S_0^{(1)}. \end{aligned}$$

Substituting these relationships into Eqs. (C.4)–(C.7) and simplifying we get the following:

$$\tilde{A} + \sum_{n=1}^N \mu^{\beta_n} \phi_{n,q}|_{q=0} T_n^{(1)} = 0, \quad (\text{C.9})$$

$$4g\mu^2(kh)^2 \chi_{m,q=1} \tilde{A} + g \sum_{n=1}^N \mu^{\beta_n} \left(4\mu^2(kh)^2 \xi_{nm} - \Lambda_{nm} \right) |_{q=1} T_n^{(1)} \\ = \mu^2(kh)^2 \left(g\chi_m - 2h\Omega_m(S_0^{(0)})^2 \sigma^2 \right) |_{q=1} \\ + g(kh)^2 \sum_{n=1}^N \mu^{\beta_n+2} (3\Phi_{nm} - 2\psi_{nm}) T_n^{(0)}, \quad m = 1 \dots N-1, \quad (\text{C.10})$$

$$\tilde{A} - (kh)S_0^{(1)} = (kh)S_0^{(0)}, \quad (\text{C.11})$$

$$gk\tilde{A} - 2\sigma^2 S_0^{(1)} + 2gk \sum_{n=1}^N \mu^{\beta_n} \psi_{nm} T_n^{(1)} \\ = \sigma^2 \left(1 - (kh)S_0^{(0)} \right) S_0^{(0)} + gk \sum_{n=1}^N \mu^{\beta_n} (R_n - G_n) |_{q=1} T_n^{(0)}. \quad (\text{C.12})$$

Note that the solutions for $T_n^{(0)}$, $S_0^{(0)}$ and σ can be found through solving Eqs. (B.15)–(B.18) from Appendix B. Solving the system of equations made up of Eqs. (C.9)–(C.12) for \tilde{A} determines an expression for the second-order nonlinear terms which can then be compared with the Stoke's second-order solution.

References

- Agnon, Y., Madsen, P.A., Schäffer, H.A., 1999. A new approach to high-order Boussinesq models. *J. Fluid Mech.* 399, 319–333. <http://dx.doi.org/10.1017/S0022112099006394> <<http://journals.cambridge.org/article/S0022112099006394>>.
- Antuono, M., Brocchini, M., 2013. Beyond Boussinesq-type equations: semi-integrated models for coastal dynamics. *Phys. Fluids* 25 (1). <http://dx.doi.org/10.1063/1.4774343> <<http://scitation.aip.org/content/aip/journal/pof2/25/1/10.1063/1.4774343>>.
- Antuono, M., Liapidevskii, V., Brocchini, M., 2009. Dispersive nonlinear shallow-water equations. *Stud. Appl. Math.* 122 (1), 1–28. <http://dx.doi.org/10.1111/j.1467-9590.2008.00422.x> <<http://dx.doi.org/10.1111/j.1467-9590.2008.00422.x>>.
- Bai, Y., Cheung, K.F., 2013. Depth-integrated free-surface flow with parameterized non-hydrostatic pressure. *Int. J. Numer. Methods Fluids* 71 (4), 403–421. <http://dx.doi.org/10.1002/fld.3664> <<http://dx.doi.org/10.1002/fld.3664>>.
- Beji, S., Battjes, J., 1993. Experimental investigation of wave propagation over a bar. *Coast. Eng.* 19 (12), 151–162. [http://dx.doi.org/10.1016/0378-3839\(93\)90022-Z](http://dx.doi.org/10.1016/0378-3839(93)90022-Z) <<http://www.sciencedirect.com/science/article/pii/037838399390022Z>>.
- Bonneton, P., Barthelmy, E., Chazel, F., Cienfuegos, R., Lannes, D., Marche, F., Tissier, M., 2011. Recent advances in Serre–Green Naghdi modelling for wave transformation, breaking and runup processes. *European Journal of Mechanics – B/Fluids*, special Issue: Nearshore Hydrodynamics 30 (6), 589–597. <http://dx.doi.org/10.1016/j.euromechflu.2011.02.005> <<http://www.sciencedirect.com/science/article/pii/S0997754611000185>>.
- Brocchini, M., 2013. A reasoned overview on Boussinesq-type models: the interplay between physics, mathematics and numerics. *Proceedings of the Royal Society A: Mathematical, Physical and Engineering Science* 469 (2160). <http://dx.doi.org/10.1098/rspa.2013.0496> <<http://rspa.royalsocietypublishing.org/content/469/2160/20130496.abstract>> <<http://rspa.royalsocietypublishing.org/content/469/2160/20130496.full.pdf+html>>.
- Casulli, V., 1999. A semi-implicit finite difference method for non-hydrostatic, free-surface flows. *Int. J. Numer. Methods Fluids* 30 (4), 425–440. [http://dx.doi.org/10.1002/\(SICI\)1097-0363\(19990630\)30:425::AID-FLD8473.0.CO;2-D](http://dx.doi.org/10.1002/(SICI)1097-0363(19990630)30:425::AID-FLD8473.0.CO;2-D) <[http://dx.doi.org/10.1002/\(SICI\)1097-0363\(19990630\)30:425::AID-FLD8473.0.CO;2-D](http://dx.doi.org/10.1002/(SICI)1097-0363(19990630)30:425::AID-FLD8473.0.CO;2-D)>.
- Casulli, V., Stelling, G., 1998. Numerical simulation of 3D quasi-hydrostatic, free-surface flows. *Journal of Hydraulic Engineering* 124 (7), 678–686. [http://dx.doi.org/10.1061/\(ASCE\)0733-9429\(1998\)124:7\(678\)](http://dx.doi.org/10.1061/(ASCE)0733-9429(1998)124:7(678)) <[http://ascelibrary.org/doi/abs/10.1061/\(ASCE\)0733-9429\(1998\)124:7\(678\)](http://ascelibrary.org/doi/abs/10.1061/(ASCE)0733-9429(1998)124:7(678))>, <[http://ascelibrary.org/doi/pdf/10.1061/\(ASCE\)0733-9429\(1998\)124:7\(678\)](http://ascelibrary.org/doi/pdf/10.1061/(ASCE)0733-9429(1998)124:7(678))>.
- Chen, Y., Liu, P.L.-F., 1995. Modified Boussinesq equations and associated parabolic models for water wave propagation. *J. Fluid Mech.* 288, 351–381. <http://dx.doi.org/10.1017/S0022112095001170> <<http://journals.cambridge.org/article/S0022112095001170>>.
- Chen, Q., Kirby, J., Dalrymple, R., Kennedy, A., Chawla, A., 2000. Boussinesq modeling of wave transformation, breaking, and runup. II: 2D. *Journal of Waterway, Port, Coastal, and Ocean Engineering* 126 (1), 48–56. [http://dx.doi.org/10.1061/\(ASCE\)0733-950X\(2000\)126:1\(39\)](http://dx.doi.org/10.1061/(ASCE)0733-950X(2000)126:1(39)) <[http://ascelibrary.org/doi/abs/10.1061/\(ASCE\)0733-950X\(2000\)126:1\(39\)](http://ascelibrary.org/doi/abs/10.1061/(ASCE)0733-950X(2000)126:1(39))>, <[http://ascelibrary.org/doi/pdf/10.1061/\(ASCE\)0733-950X\(2000\)126:1\(39\)](http://ascelibrary.org/doi/pdf/10.1061/(ASCE)0733-950X(2000)126:1(39))>.
- Cienfuegos, R., Barthelmy, E., Bonneton, P., 2007. A fourth-order compact finite volume scheme for fully nonlinear and weakly dispersive Boussinesq-type equations. Part II: boundary conditions and validation. *Int. J. Numer. Methods*

- Fluids* 53 (9), 1423–1455. <http://dx.doi.org/10.1002/fld.1359> <<http://dx.doi.org/10.1002/fld.1359>>.
- Dean, R.G., Dalrymple, R.A., 1991. *Water Wave Mechanics for Engineers and Scientists*. World Scientific.
- Dingemans, M., 1994. Comparison of computations with Boussinesq-like models and laboratory measurements. *Report H-1684.12* 32.
- Do Carmo, J.S.A., Santos, F.J.S., Barthlemy, E., 1993. Surface waves propagation in shallow water: A finite element model. *Int. J. Numer. Methods Fluids* 16 (6), 447–459. <http://dx.doi.org/10.1002/fld.1650160602> <<http://dx.doi.org/10.1002/fld.1650160602>>.
- Dommermuth, D., 2000. The initialization of nonlinear waves using an adjustment scheme. *Wave Motion* 32 (4), 307–317. [http://dx.doi.org/10.1016/S0165-2125\(00\)00047-0](http://dx.doi.org/10.1016/S0165-2125(00)00047-0) <<http://www.sciencedirect.com/science/article/pii/S0165212500000470>>.
- Erduran, K.S., Ilic, S., Kutija, V., 2005. Hybrid finite-volume finite-difference scheme for the solution of Boussinesq equations. *Int. J. Numer. Methods Fluids* 49 (11), 1213–1232. <http://dx.doi.org/10.1002/fld.1021> <<http://dx.doi.org/10.1002/fld.1021>>.
- Ertekin, R.C., Wehausen, J.V., 1986. Some soliton calculations. In: *Proc. 16th Symp. Naval Hydrodynamics*, p. 167.
- Gallerano, F., Cannata, G., Villani, M., 2014. An integral contravariant formulation of the fully non-linear Boussinesq equations. *Coast. Eng.* 83, 119–136. <http://dx.doi.org/10.1016/j.coastaleng.2013.09.006> <<http://www.sciencedirect.com/science/article/pii/S0378383913001567>>.
- Gobbi, M.F., Kirby, J.T., 2001. A fourth order Boussinesq-type wave model. *Coast. Eng. Proc.* 1 (25) <<http://journals.tdl.org/icce/index.php/icce/article/view/5291>>.
- Gobbi, M.F., Kirby, J.T., 1999. Wave evolution over submerged sills: tests of a high-order Boussinesq model. *Coast. Eng.* 37 (1), 57–96. [http://dx.doi.org/10.1016/S0378-3839\(99\)00015-0](http://dx.doi.org/10.1016/S0378-3839(99)00015-0) <<http://www.sciencedirect.com/science/article/pii/S0378383999000150>>.
- Gobbi, M.F., Kirby, J.T., Wei, G., 2000. A fully nonlinear Boussinesq model for surface waves. part 2. extension to $O(kh)^4$. *J. Fluid Mech.* 405, 181–210. <http://dx.doi.org/10.1017/S0022112099007247> <<http://journals.cambridge.org/article/S0022112099007247>>.
- Green, A.E., Naghdi, P.M., 1976. A derivation of equations for wave propagation in water of variable depth. *J. Fluid Mech.* 78, 237–246. <http://dx.doi.org/10.1017/S0022112076002425> <<http://journals.cambridge.org/article/S0022112076002425>>.
- Grosso, G., Antuono, M., Brocchini, M., 2010. Dispersive nonlinear shallow-water equations: some preliminary numerical results. *J. Eng. Math.* 67 (1–2), 71–84. <http://dx.doi.org/10.1007/s10665-009-9328-5> <<http://dx.doi.org/10.1007/s10665-009-9328-5>>.
- Johnson, R., 1973. On the development of a solitary wave moving over an uneven bottom. *Proceedings of the Cambridge Philosophical Society*, vol. 73. Cambridge University Press, pp. 183–203.
- Kennedy, A.B., Fenton, J.D., 1997. A fully-nonlinear computational method for wave propagation over topography. *Coast. Eng.* 32 (23), 137–161. [http://dx.doi.org/10.1016/S0378-3839\(97\)81747-4](http://dx.doi.org/10.1016/S0378-3839(97)81747-4) <<http://www.sciencedirect.com/science/article/pii/S0378383997817474>>.
- Kennedy, A., Chen, Q., Kirby, J., Dalrymple, R., 2000. Boussinesq modeling of wave transformation, breaking, and runup. I: 1D. *Journal of Waterway, Port, Coastal, and Ocean Engineering* 126 (1), 39–47. [http://dx.doi.org/10.1061/\(ASCE\)0733-950X\(2000\)126:1\(39\)](http://dx.doi.org/10.1061/(ASCE)0733-950X(2000)126:1(39)) <[http://ascelibrary.org/doi/abs/10.1061/\(ASCE\)0733-950X\(2000\)126:1\(39\)](http://ascelibrary.org/doi/abs/10.1061/(ASCE)0733-950X(2000)126:1(39))>, <[http://ascelibrary.org/doi/pdf/10.1061/\(ASCE\)0733-950X\(2000\)126:1\(39\)](http://ascelibrary.org/doi/pdf/10.1061/(ASCE)0733-950X(2000)126:1(39))>.
- Kennedy, A.B., Kirby, J.T., Chen, Q., Dalrymple, R.A., 2001. Boussinesq-type equations with improved nonlinear performance. *Wave Motion* 33 (3), 225–243. [http://dx.doi.org/10.1016/S0165-2125\(00\)00071-8](http://dx.doi.org/10.1016/S0165-2125(00)00071-8) <<http://www.sciencedirect.com/science/article/pii/S0165212500000718>>.
- Li, Y., Liu, S.-X., Yu, Y.-X., Lai, G.-Z., 1999. Numerical modeling of Boussinesq equations by finite element method. *Coast. Eng.* 37 (2), 97–122. [http://dx.doi.org/10.1016/S0378-3839\(99\)00014-9](http://dx.doi.org/10.1016/S0378-3839(99)00014-9) <<http://www.sciencedirect.com/science/article/pii/S0378383999000149>>.
- Lynett, P., Liu, P.L., 2004a. A two-layer approach to wave modelling. *Proc. Roy. Soc. Lond. Ser. A: Math. Phys. Eng. Sci.* 460 (2049), 2637–2669. <http://dx.doi.org/10.1098/rspa.2004.1305> <<http://rspa.royalsocietypublishing.org/content/460/2049/2637.abstract>>, <<http://rspa.royalsocietypublishing.org/content/460/2049/2637.full.pdf+html>>.
- Lynett, P.J., Liu, P.L.-F., 2004b. Linear analysis of the multi-layer model. *Coast. Eng.* 51 (56), 439–454. <http://dx.doi.org/10.1016/j.coastaleng.2004.05.004> <<http://www.sciencedirect.com/science/article/pii/S0378383904000560>>.
- Lynett, P.J., Wu, T.-R., Liu, P.L.-F., 2002. Modeling wave runup with depth-integrated equations. *Coast. Eng.* 46 (2), 89–107. [http://dx.doi.org/10.1016/S0378-3839\(02\)00043-1](http://dx.doi.org/10.1016/S0378-3839(02)00043-1) <<http://www.sciencedirect.com/science/article/pii/S0378383902000431>>.
- Madsen, P.A., Agnon, Y., 2003. Accuracy and convergence of velocity formulations for water waves in the framework of Boussinesq theory. *J. Fluid Mech.* 477, 285–319. <http://dx.doi.org/10.1017/S0022112002003257> <<http://journals.cambridge.org/article/S0022112002003257>>.
- Madsen, O.S., Mei, C.C., 1969. The transformation of a solitary wave over an uneven bottom. *J. Fluid Mech.* 39, 781–791. <http://dx.doi.org/10.1017/S0022112069002461> <<http://journals.cambridge.org/article/S0022112069002461>>.
- Madsen, P.A., Schäffer, H.A., 1998. Higher-order Boussinesq-type equations for surface gravity waves: derivation and analysis. *Philosophical Transactions of the Royal Society of London. Series A: Mathematical, Physical and Engineering*

- Sciences 356 (1749), 3123–3181. <http://dx.doi.org/10.1098/rsta.1998.0309> <<http://rsta.royalsocietypublishing.org/content/356/1749/3123.abstract>>, <<http://rsta.royalsocietypublishing.org/content/356/1749/3123.full.pdf+html>>.
- Madsen, P.A., Srensen, O.R., 1992. A new form of the Boussinesq equations with improved linear dispersion characteristics. Part 2. a slowly-varying bathymetry. *Coast. Eng.* 18 (34), 183–204. [http://dx.doi.org/10.1016/0378-3839\(92\)90019-Q](http://dx.doi.org/10.1016/0378-3839(92)90019-Q) <<http://www.sciencedirect.com/science/article/pii/037838399290019Q>>.
- Madsen, P., Srensen, O., 1993. Bound waves and triad interactions in shallow water. *Ocean Eng.* 20 (4), 359–388. [http://dx.doi.org/10.1016/0029-8018\(93\)90002-Y](http://dx.doi.org/10.1016/0029-8018(93)90002-Y) <<http://www.sciencedirect.com/science/article/pii/002980189390002Y>>.
- Madsen, P.A., Murray, R., Srensen, O.R., 1991. A new form of the Boussinesq equations with improved linear dispersion characteristics. *Coast. Eng.* 15 (4), 371–388. [http://dx.doi.org/10.1016/0378-3839\(91\)90017-B](http://dx.doi.org/10.1016/0378-3839(91)90017-B) <<http://www.sciencedirect.com/science/article/pii/037838399190017B>>.
- Ma, G., Shi, F., Kirby, J.T., 2012. Shock-capturing non-hydrostatic model for fully dispersive surface wave processes. *Ocean Modell.* 4344, 22–35. <http://dx.doi.org/10.1016/j.ocemod.2011.12.002> <<http://www.sciencedirect.com/science/article/pii/S1463500311001892>>.
- Nwogu, O., 1993. Alternative form of Boussinesq equations for nearshore wave propagation. *J. Waterway Port Coast. Ocean Eng.* 119 (6), 618–638. [http://dx.doi.org/10.1061/\(ASCE\)0733-950X\(1993\)119:6\(618\)](http://dx.doi.org/10.1061/(ASCE)0733-950X(1993)119:6(618)) <<http://ascelibrary.org/doi/abs/10.1061/%28ASCE%290733-950X%281993%29119%3A6%28618%29%29>>, <<http://ascelibrary.org/doi/pdf/10.1061/%28ASCE%290733-950X%281993%29119%3A6%28618%29%29>>.
- Panda, N., Dawson, C., Zhang, Y., Kennedy, A.B., Westerink, J.J., Donahue, A.S., 2014. Discontinuous Galerkin methods for solving Boussinesq–Green–Naghdi equations in resolving non-linear and dispersive surface water waves. *J. Comput. Phys.* 273, 572–588. <http://dx.doi.org/10.1016/j.jcp.2014.05.035> <<http://www.sciencedirect.com/science/article/pii/S0021999114003982>>.
- Peregrine, D.H., 1967. Long waves on a beach. *J. Fluid Mech.* 27, 815–827. <http://dx.doi.org/10.1017/S00222112067002605> <<http://journals.cambridge.org/article/S00222112067002605>>.
- Roerber, V., Cheung, K.F., Kobayashi, M.H., 2010. Shock-capturing Boussinesq-type model for nearshore wave processes. *Coast. Eng.* 57 (4), 407–423. <http://dx.doi.org/10.1016/j.coastaleng.2009.11.007> <<http://www.sciencedirect.com/science/article/pii/S0378383909001860>>.
- Schäffer, H.A., Madsen, P.A., 1995. Further enhancements of Boussinesq-type equations. *Coast. Eng.* 26 (12), 1–14. [http://dx.doi.org/10.1016/0378-3839\(95\)00017-2](http://dx.doi.org/10.1016/0378-3839(95)00017-2) <<http://www.sciencedirect.com/science/article/pii/0378383995000172>>.
- Schäffer, H.A., Madsen, P.A., Deigaard, R., 1993. A Boussinesq model for waves breaking in shallow water. *Coast. Eng.* 20 (34), 185–202. [http://dx.doi.org/10.1016/0378-3839\(93\)90001-O](http://dx.doi.org/10.1016/0378-3839(93)90001-O) <<http://www.sciencedirect.com/science/article/pii/037838399390001O>>.
- Serre, F., 1953. Contribution à l'étude des écoulements permanents et variables dans les canaux. *La Houille Blanche* 3, 374–388. <http://dx.doi.org/10.1051/lhb/1953034> <<http://dx.doi.org/10.1051/lhb/1953034>>.
- Shi, F., Kirby, J.T., Harris, J.C., Geiman, J.D., Grilli, S.T., 2012. A high-order adaptive time-stepping TVD solver for Boussinesq modeling of breaking waves and coastal inundation. *Ocean Modell.* 4344, 36–51. <http://dx.doi.org/10.1016/j.ocemod.2011.12.004> <<http://www.sciencedirect.com/science/article/pii/S1463500311002010>>.
- Stansby, P.K., Zhou, J.G., 1998. Shallow-water flow solver with non-hydrostatic pressure: 2D vertical plane problems. *Int. J. Numer. Methods Fluids* 28 (3), 541–563. [http://dx.doi.org/10.1002/\(SICI\)1097-0363\(19980915\)28:3541::AID-FLD7383.0.CO;2-0](http://dx.doi.org/10.1002/(SICI)1097-0363(19980915)28:3541::AID-FLD7383.0.CO;2-0) <[http://dx.doi.org/10.1002/\(SICI\)1097-0363\(19980915\)28:3541::AID-FLD7383.0.CO;2-0](http://dx.doi.org/10.1002/(SICI)1097-0363(19980915)28:3541::AID-FLD7383.0.CO;2-0)>.
- Stelling, G., Zijlema, M., 2003. An accurate and efficient finite-difference algorithm for non-hydrostatic free-surface flow with application to wave propagation. *Int. J. Numer. Methods Fluids* 43 (1), 1–23. <http://dx.doi.org/10.1002/flid.595> <<http://dx.doi.org/10.1002/flid.595>>.
- Wei, Z., Jia, Y., 2013. A depth-integrated non-hydrostatic finite element model for wave propagation. *Int. J. Numer. Methods Fluids* 73 (11), 976–1000. <http://dx.doi.org/10.1002/flid.3832> <<http://dx.doi.org/10.1002/flid.3832>>.
- Wei, G., Kirby, J., 1995. Time-dependent numerical code for extended Boussinesq equations. *J. Waterway Port Coastal Ocean Eng.* 121 (5), 251–261. [http://dx.doi.org/10.1061/\(ASCE\)0733-950X\(1995\)121:5\(251\)](http://dx.doi.org/10.1061/(ASCE)0733-950X(1995)121:5(251)) <[http://dx.doi.org/10.1061/\(ASCE\)0733-950X\(1995\)121:5\(251\)](http://dx.doi.org/10.1061/(ASCE)0733-950X(1995)121:5(251))>, <[http://dx.doi.org/10.1061/\(ASCE\)0733-950X\(1995\)121:5\(251\)](http://dx.doi.org/10.1061/(ASCE)0733-950X(1995)121:5(251))>.
- Wei, G., Kirby, J.T., Grilli, S.T., Subramanya, R., 1995. A fully nonlinear Boussinesq model for surface waves. Part 1. Highly nonlinear unsteady waves. *J. Fluid Mech.* 294, 71–92. <http://dx.doi.org/10.1017/S0022112095002813> <<http://journals.cambridge.org/article/S0022112095002813>>.
- Willmott, C.J., 1981. On the validation of models. *Physical Geography* 2 (2), 184–194. <http://dx.doi.org/10.1080/02723646.1981.10642213> <<http://www.tandfonline.com/doi/abs/10.1080/02723646.1981.10642213>>, <<http://www.tandfonline.com/doi/pdf/10.1080/02723646.1981.10642213>>.
- Yamazaki, Y., Kowalik, Z., Cheung, K.F., 2009. Depth-integrated, non-hydrostatic model for wave breaking and run-up. *Int. J. Numer. Methods Fluids* 61 (5), 473–497. <http://dx.doi.org/10.1002/flid.1952> <<http://dx.doi.org/10.1002/flid.1952>>.
- Zhang, Y., Kennedy, A.B., Panda, N., Dawson, C., Westerink, J.J., 2013. Boussinesq–Green–Naghdi rotational water wave theory. *Coast. Eng.* 73, 13–27. <http://dx.doi.org/10.1016/j.coastaleng.2012.09.005> <<http://www.sciencedirect.com/science/article/pii/S037838391200155X>>.
- Zhang, Y., Kennedy, A.B., Donahue, A.S., Westerink, J.J., Panda, N., Dawson, C., 2014. Rotational surf zone modeling for Boussinesq–Green–Naghdi systems. *Ocean Modell.* 79, 43–53. <http://dx.doi.org/10.1016/j.ocemod.2014.04.001> <<http://www.sciencedirect.com/science/article/pii/S1463500314000419>>.
- Zhang, Y., Kennedy, A.B., Panda, N., Dawson, C., Westerink, J.J., 2014. Generating-absorbing sponge layers for phase-resolving wave models. *Coast. Eng.* 84, 1–9. <http://dx.doi.org/10.1016/j.coastaleng.2013.10.019> <<http://www.sciencedirect.com/science/article/pii/S0378383913001750>>.
- Zijlema, M., Stelling, G.S., 2005. Further experiences with computing non-hydrostatic free-surface flows involving water waves. *Int. J. Numer. Methods Fluids* 48 (2), 169–197. <http://dx.doi.org/10.1002/flid.821> <<http://dx.doi.org/10.1002/flid.821>>.
- Zijlema, M., Stelling, G., 2008. Efficient computation of surf zone waves using the nonlinear shallow water equations with non-hydrostatic pressure. *Coast. Eng.* 55 (10), 780–790. <http://dx.doi.org/10.1016/j.coastaleng.2008.02.020> <<http://www.sciencedirect.com/science/article/pii/S0378383908000380>>.
- Zijlema, M., Stelling, G., Smit, P., 2011. SWASH: An operational public domain code for simulating wave fields and rapidly varied flows in coastal waters. *Coast. Eng.* 58 (10), 992–1012. <http://dx.doi.org/10.1016/j.coastaleng.2011.05.015> <<http://www.sciencedirect.com/science/article/pii/S0378383911000974>>.